# Magnetic states and phase transitions in frustrated triangular-lattice antiferromagnets

R. S. Gekht

*L. V. Kirenski Institute of Physics, Siberian Branch of the Academy of Sciences of the USSR, Krasnoyarsk*
Usp. Fiz. Nauk **159**, 261–296 (October 1989)

Recent experimental and theoretical investigations of frustrated triangular-lattice antiferromagnets are reviewed. An analysis is made of phases with different structures: partly disordered and double incommensurate states, helical configurations, triangular superstructures, etc. These phases appear because of an instability of the conical high-symmetry point in the Brillouin zone as a result of the dipole interaction, or they may be due to other factors. An analysis is made of magnetic transitions belonging to new universal classes as well as Berezinskiĭ–Kosterlitz–Thouless transitions with an exponential decay of correlations in the low-temperature phase. The chiral symmetry and the associated problem of transition accompanied by simultaneous ordering of discrete and continuous components of the order parameter space are considered for triangular antiferromagnets with different spins. The spectrum of collective modes of some incommensurate structures is analyzed.

## 1. INTRODUCTION

It is well known that frustration effects play an important role in various magnetic systems. In particular, triangular-lattice antiferromagnets are a typical example of such frustrated spin systems. Recent experimental and theoretical investigations have made it possible to establish that they manifest many properties which do not agree with the current models of nonfrustrated materials. This difference is manifested primarily by a wide range of phases and phase transitions, which is the result of a strong degeneracy leading to a high sensitivity of such systems to various perturbations.

For example, measurements of thermal and magnetic properties[1] and neutron diffraction investigations[2] of the triangular antiferromagnet $RbFeCl_3$ have revealed that instead of a direct transition from the paraelectric to the commensurate phase, there are two intermediate (on the temperature scale) incommensurate phases. Moreover, these very interesting results have revealed a new incommensurate structure in which the periods of the two magnetization components are incommensurate with the lattice period and in relation to one another. As pointed out by Shiba,[3] incommensurate phases in frustrated antiferromagnetic $RbFeCl_3$ appear because of a new mechanism which is due to an instability of the high-symmetry conical point resulting from a weak dipole interaction. This instability of the conical point can be induced by an external field[4–6] even in the case of such triangular magnetic materials as $CsNiF_3$, $CsFeCl_3$, and $CsCuCl_3$, when in $H=0$ there are no incommensurate phases or where they appear due to a different mechanism.[7,8]

In the case of other substances, such as transition metal halides,[10,11] the experimentally observed behavior is different: The modulated-phase period increases with the temperature $T$ of a sample and a transition takes place to a commensurate intermediate state. The point of transition between different ordered states can then vary in a wide range of temperatures $T$ both under pressure[12] and because of partial replacement of some nonmagnetic ions with others.[13] The nonlinear mechanism of the variation of the structure wave vector with $T$, related to a generation of higher harmonics, is not observed in the case of these materials, but in their case it is important to allow for the thermal renormalization of the exchange constants,[14] which leads to an increase in the mode period with temperature.[15]

Frustrations in rhombohedral antiferromagnets are possible both in one plane and in a third direction. If frustrations exist simultaneously along all three directions, then systems of this kind (for example, the $\beta$ phase of oxygen) have helical structures exhibiting continuous degeneracy in respect of the wave vector direction and magnitude.[48,49]

Ising frustrated antiferromagnets $CsCoCl_3$ and $CsCoBr_3$ exhibit anomalies of physical properties at two temperatures.[16,17] Calculations carried out using the mean field approximation[18] and also the cluster variational method[19] demonstrate that one of the magnetic sublattices is disordered in an intermediate state. The Monte Carlo method has been used[20,21] and it has been found that such partly ordered states are described by a mode with a phase which varies randomly in space and in time. These results can account for the considerable fluctuations of the magnetic structure with time exhibited by $CsCoCl_3$ crystals.[16]

Coupling between transverse components of the spins in Ising-like Heisenberg antiferromagnets stimulates ordering of the magnetic sublattices. Therefore, cooling of these compounds induces order of the longitudinal components of the spins in all three sublattices. Moreover, further cooling ensures additional ordering of the transverse components.[44] It is interesting to note that in the limiting case of $T=0$ we can expect nontrivial degeneracy of the ground state: The angles between the three magnetic sublattices may vary but the total angular momentum can still remain nonzero (and direction-degenerate); this state is not disturbed even by linear excitations.

In isotropic and $XY$-like antiferromagnets the angles between the sublattices are fixed and amount to 120°. The compounds with 120° structures have been known for some time.[23,24] Nevertheless, some new and interesting results obtained recently for these systems (characterized by an extremely simple fundamental interaction) have not been mentioned in any reviews. The properties of the phases and the nature of the ordering process in these structures is in many respects unusual, as found—for example—in the case of two-dimensional frustrated antiferromagnetics with the Heisenberg or $XY$ spins. Thus, in the case of an isotropic

 0038-5670/89/100871-20$01.80  

Heisenberg antiferromagnet a phase transition occurs even in zero external field, and in a low-temperature phase the spin correlations decay exponentially (in the same way as in a high-temperature phase). These two phases are distinguished qualitatively by Kawamura and Miyashita[22] in terms of a vortex function introduced by them: This function is an analog of the Wilson loop in the problem of quark confinement in the lattice gauge theory.[29,30] Interesting experimental data on such systems have been obtained recently[31-34] for a series of $VX_2$ compounds (where X = Cl, Br, I). Triangular $XY$ antiferromagnets are characterized by continuous and doubly discrete symmetries. Nevertheless, in zero magnetic field these systems exhibit in practice a single continuous transition because the interaction between two possible types of topological defects (walls and vortices) results in coalescence (or at least extreme proximity) of the critical points corresponding to the Ising and Berezinskiĭ–Kosterlitz–Thouless transitions.

Quantum effects are very important in frustrated spin $S = 1/2$ antiferromagnets. Back in 1973 Anderson demonstrated[45] that a magnetic quantum liquid may exist in Heisenberg antiferromagnets and the ground state of this liquid can be regarded as representing an ensemble of randomly distributed singlet pairs on a triangular lattice. Recent experimental investigations of a sample of $NaTiO_2$ confirmed[46] the absence of ordered states and phase transitions in systems with $S = 1/2$. In the case of Ising-like Heisenberg antiferromagnets ($S = 1/2$) there are spin configurations analogous to the classical ones and they exist in a certain range of external fields,[47] whereas in the case of $XY$ antiferromagnets the correlation function shows a gradual decay at $T = 0$ (Ref. 36).

Recent experimental and theoretical investigations have enabled us to understand many interesting and unexpected properties of the systems under consideration with a distinguishing feature of a high sensitivity to the type of interaction (this is due to the frustration effects). We shall first consider the likely structures and the behavior of the spectrum of collective modes in systems with the dipole interaction (Sec. 2). The substances with intermediate phases which can be described in terms of the conical point instability include $AFeCl_3$ compounds (A = Rb, Cs, Tl, $NH_3$); in the case of these compounds the triangular lattices are formed from ferromagnetic chains and the exchange interaction within these chains is much stronger than the antiferromagnetic interaction between them. An instability of the high-symmetry point may also be observed in substances formed from antiferromagnetic chains. However, in contrast to those with ferromagnetic chains, the dipole interaction is now an order of magnitude less,[56] so that the temperature ranges where incommensurate phases are observed (if they exist at all) are much narrower. In Sec. 2 we shall consider in detail all possible phases of compounds $RbFeCl_3$ and $CsFeCl_3$, and also of compounds isomorphous with them, such as $CsNiF_3$ and $CsCuCl_3$.

Then, in Sec. 3 we shall consider frustrated antiferromagnets exhibiting a planar helical (spiral) state. In the case of rhombohedral antiferromagnets of the $NiBr_2$ type the state with a spiral appears only at low temperatures, whereas in the intermediate range there is a commensurate antiferromagnetic state. In the case of other rhombohedral compounds (of the $\beta$-$O_2$ type) a commensurate intermediate state is absent and a state with a spiral exists throughout the temperature range below the point of transition from the paraelectric phase. At these intermediate temperatures there is a continuously degenerate state with inequivalent spirals, whereas at low temperatures where quantum fluctuations are important, there is a state with a fixed wave vector of the spiral.[37] The same Sec. 3 deals with Ising frustrated antiferromagnets in the presence of additional exchange interactions between the second-nearest spins ($CsCoCl_3$, $CsCoBr_3$). Ising frustrated systems may also have triangular-superstructure states.[51]

Transitions with all possible types of symmetry breaking in two-dimensional triangular antiferromagnets are considered in Sec. 4. The latter include both Heisenberg paramagnets of the $VCl_2$ type with $S = 3/2$, as well as magnetic substances such as $NaTiO_2$ and $LiNiO_2$ with $S = 1/2$. They all exhibit an extremely weak interplanar exchange interaction. The results of theoretical investigations are compared in this section with the available experimental data for a planar quasi-two-dimensional antiferromagnet $CsMnBr_3$ (Ref. 111). The review ends (Sec. 5) with a brief discussion of future research trends.

## 2. INCOMMENSURATE STATES DUE TO THE DIPOLE INTERACTION IN TRIANGULAR ANTIFERROMAGNETS

### 2.1. Instability of the conical high-symmetry point of triangular antiferromagnet $RbFeCl_3$. Phases with a double incommensurate structure

Incommensurate magnetic structures usually appear in crystals with competition between the positive and negative coupling of the nearest to the second-nearest spins or when the lattice symmetry admits the existence of the Lifshitz invariants in the expansion describing the free energy.[7,8] However, frustrated triangular lattices may form modulated phases due to a new mechanism related closely to degeneracy of the conical high-symmetry point $K$ in the Brillouin zone.[52] In the case of frustrated antiferromagnets of the $RbFeCl_3$ type the degeneracy at the high-symmetry point $K$ may be lifted because of the dipole interaction.[3] This gives rise not only to simple incommensurate phases, but also to phases with an unusual double incommensurate structure found experimentally in $RbFeCl_3$ (Refs. 1 and 2).

The compound $RbFeCl_3$ is an hexagonal magnetic material with the crystal structure characterized by the space symmetry group $D^4_{6h}$. The $Fe^{2+}$ magnetic ions with $XY$-like spins are situated along the $c$ axis giving rise to a triangular lattice. An exchange antiferromagnetic coupling $J_0$ is established along the chains of these compounds, whereas a weaker antiferromagnetic coupling $J_1$ applies between the chains. The antiferromagnetic interaction in a triangular lattice gives rise to a 120° structure consisting of three magnetic sublattices (Fig. 1a). If we allow for the dipole forces, even when they are much smaller than the exchange couplings $J_0$ and $J_1$, such a structure should not form at the temperature $T_1$ of the transition from the paraelectric phase: quite different spin configurations appear instead of it at intermediate temperatures $T$.

In fact, below the instability point $T_1$ the wave vector $\mathbf{Q}$ of the condensing mode corresponds to the smallest eigenvalue of the Fourier component of the interchain exchange and dipole interactions

$$A_{\alpha\beta}(\mathbf{Q}) = J(\mathbf{Q})\delta_{\alpha\beta} + D_{\alpha\beta}(\mathbf{Q}); \qquad (2.1)$$

here,

$$J(\mathbf{Q}) = -2J_1[\cos(\mathbf{Qa}) + \cos(\mathbf{Qb}) + \cos(\mathbf{Q}(\mathbf{a}-\mathbf{b}))] \quad (J_1 < 0), \qquad (2.2)$$

where $\mathbf{a} = a(1,0,0)$ and $\mathbf{b} = a(1/2,\sqrt{3}/2,0)$ are the fundamental translation vectors in the basal plane of the hexagonal lattice. A minimum of the function $J(\mathbf{Q})$ occurs at a point $K$ in the reciprocal lattice space and this point corresponds to $\mathbf{Q} = \mathbf{Q}_K \equiv (4\pi/3a,0,0)$. Contrary to $J(\mathbf{Q})$, calculations of the dipole tensor $D_{\alpha\beta}(\mathbf{Q})$, carried out by the Ewald method,[53] show that after expansion as a series near the point $K$ it contains terms which are linear in $\mathbf{q} = \mathbf{Q} - \mathbf{Q}_k$:

$$D_{xx} = \gamma_d(\xi - \eta q_x), \qquad D_{xy} = \gamma_d \eta q_y \qquad (2.3)$$

[$\gamma_d = (g\mu_B)^2/a^3$; $\xi$ and $\eta$ are numerical constants depending on the lattice constants $c$ and $a$; $D_{yy}$ differs from $D_{xx}$ by a change of the sign in front of the term containing $q_x$]. Therefore, the smallest eigenvalue $\lambda_-(\mathbf{Q})$ of the matrix $A_{\alpha\beta}(\mathbf{Q})$ is localized not at $\mathbf{Q} = \mathbf{Q}_k$, but in the vicinity of the point $K$. The eigenvalues $\lambda_\pm(\mathbf{Q})$ of the matrix (2.1) are shown in Fig. 1b: two potential surfaces $\lambda_+$ and $\lambda_-$ intersect at the conical point $K$.[1)] Figure 1c shows the equipotential lines of the lower branch near the point $K$, as well as the spin polarization along the contour shown by the dashed curve. Minima of $\lambda_-(\mathbf{Q})$ are located at three equivalent points[56] with the value $Q = Q_1$, where the eigenvectors are polarized parallel to the wave vectors of the $\mathbf{q} = \mathbf{Q}_1 - \mathbf{Q}_k$ type. The points at the minima are separated from one another by a barrier and the maximum value of the barrier height is found at saddle points where $q_2 = |\mathbf{Q}_2 - \mathbf{Q}_k|$. At these points we have a different situation: the eigenvectors are polarized orthogonally to vectors of the $\mathbf{q}_2$ type. The presence of such singularities in the spectrum of $\lambda_-(\mathbf{Q})$ not only makes possible formation of a longitudinal modulation wave with $\mathbf{q}_1$ below the instability point of the symmetric phase $T_1$, but also allows formation of an additional transverse wave $\mathbf{q}_2$ at lower temperatures, when the value of the average angular momentum becomes quite large.

An increase in the ratio $\gamma_d/|J_1|$ shifts the position of $Q_1$ in Fig. 1c from the point $K$ to the point $M$, which corresponds to the antiparallel orientation of the spins.

We shall now consider consecutive phase transitions applying the Landau expansion to the free energy, accurate to within terms of the fourth order in respect of the magnetization $M_\alpha$ ($\alpha = x, y$):

$$F = \int d\mathbf{R}\left[\frac{1}{2}\sum_{\alpha,\beta} M_\alpha(\mathbf{R})\, a_{\alpha\beta}(-i\nabla)\, M_\beta(\mathbf{R}) + b\left(\sum_\alpha M_\alpha^2(\mathbf{R})\right)^2\right] \quad (b > 0). \qquad (2.4)$$

Since in the case $\gamma_d \ll |J'|$ the wave vector lies in the vicinity of the point $K$, it is convenient to express $M_\alpha$ in the form

$$M_\alpha(\mathbf{R}) = \psi_\alpha(\mathbf{R})\exp(i\mathbf{Q}_k\mathbf{R}) + \text{c.c.}, \qquad (2.5)$$

where the complex variables $\psi_\alpha$ are the components of the order parameter. After substitution of Eq. (2.5) into Eq. (2.4), the free energy can be expressed in terms of $\psi_\alpha$ as follows[56]:

$$F = \int d\mathbf{R}\left\{\sum_{\alpha,\beta}\psi_\alpha^* a_{\alpha\beta}(\mathbf{Q}_k - i\nabla)\psi_\beta + b[4(|\psi_x|^2 + |\psi_y|^2)^2 + 2(\psi_x^2 + \psi_y^2)^*(\psi_x^2 + \psi_y^2)]\right\}, \qquad (2.6)$$

where $a_{\alpha\beta}(\mathbf{Q}) = A_{\alpha\beta}(\mathbf{Q}) + \alpha T\delta_{\alpha\beta}$ is the reciprocal susceptibility tensor ($\alpha > 0$). An analysis of possible structures on the basis of Eq. (2.6) shows that cooling induces consecutive phase transitions to three different states. First of all, at an instability point $T_1$ of the magnetic phase a partly ordered state appears: It has one spin component and is characterized by

$$\psi_x^0(x) = \varphi_0 \exp(iq_1^0 x),$$
$$|\varphi_0| = [\alpha(T_1 - T)(12b)^{-1}]^{1/2}, \qquad (2.7)$$
$$q_1^0 = \frac{2}{3}\frac{\gamma_d\eta}{|J_1|}.$$

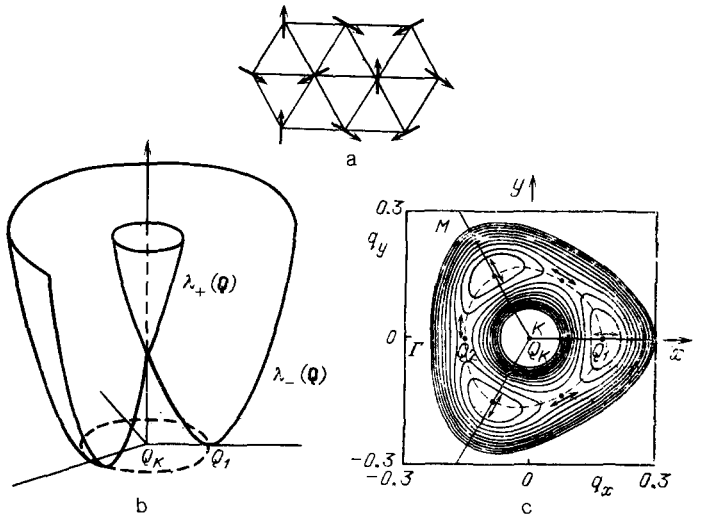


FIG. 1. a) Ground state of a triangular antiferromagnet, 120° structure. b) Eigenvalues $\lambda_\pm(\mathbf{Q})$ of the potential surface in the vicinity of the high-symmetry point $\mathbf{Q}_k$. c) Equipotential lines representing $\lambda_-(\mathbf{Q})$; $\mathbf{Q}_1$ and two other equivalent points correspond to the minimum of $\lambda_-(\mathbf{Q})$. The arrows on the dashed contour indicate the spin polarization.[56]

At lower temperatures—below a point $T_2$—the thermodynamic state has two ordered spin components. In this case we can expect not only a longitudinal modulation wave, but also a transverse wave $\psi_y^0 = \varphi_y^{(0)} \exp(iq_2^0 x)$, where

$$|\varphi_y^{(0)}|^2 = -[3a_{yy}(\mathbf{Q}_2) - 2a_{xx}(\mathbf{Q}_1)](20b)^{-1}. \quad (2.8)$$

[The amplitude $\varphi_x^{(0)}$ of the longitudinal wave $\psi_x^0 = \varphi_x^{(0)} \exp(iq_1^0 x)$ is obtained after replacing the subscripts $x, y$ and 1, 2 in Eq. (2.8) with $y, x$ and 2, 1, respectively.] In the state characterized by $q_1^0$ and $q_2^0$ the two spin projections have different periods and these periods are incommensurate with the lattice period and also relative to one another. This type of magnetic ordering is new and it reflects the anisotropic nature of the dipole interaction (and also the fact that the double incommensurate structure could not exist in principle without an instability of the conical high-symmetry point induced by the dipole forces).

At even lower temperatures, when a critical point $T_3$ is reached, there is finally a transition to a commensurate 120° state; in this three-sublattice state the complex amplitudes are related by $\psi_y^0 = \pm i\psi_x^0$.

It follows from neutron diffraction investigations[2] of $RbFeCl_3$ that it exhibits three phase transitions at 2.5, 2.35, and 1.95 K, and that the spin polarizations of two incommensurate structures agree with the above theory. At 2.5 K the experimental values $q_1 = q_1^0$ for the longitudinal modulation wave amount to[2] $0.16\,a^{-1}$, whereas the values of $q_2 = q_2^0$ for the transverse wave are[2] $0.11\,a^{-1}$ at $T = 2.3$ K. These results are close to the theoretical values[3]: $q_1^0 = 2\eta\gamma_d/3|J_1| = 0.18a^{-1}$ (we are assuming here that $\gamma_d = 0.027$ K, $J_1 = -0.5$ K, $\eta = 5$) and $q_2^0 = 0.15a^{-1}$.

### 2.2. Amplitude and phase modulations. Collective modes in $RbFeCl_3$

In an intermediate state, when only one spin component is ordered, the period of the longitudinal modulation wave and its sinusoidal profile are not affected by cooling. However, after transition to a state in which both spin components are ordered, the experimental results reported for $RbFeCl_3$ indicate a temperature dependence of the wave vectors of the modes.[2] The mechanism responsible for the temperature dependences is the interaction of the longitudinal and transverse modes, which lowers additionally the free energy. The nonlinear relationship in Eq. (2.6)—represented by the cross terms $(\psi_x^0\psi_y^{0*})^2$ and $(\psi_x^{0*}\psi_y^0)^2$—leads to a change from a purely sinusoidal structure to a soliton one on increase in the intensities of the induced harmonics. The resultant configurations are characterized not only by a spatial variation of the phase, but generally also by spatial changes in the amplitude of a nonlinear wave.[73]

The general solution of the equations obtained on variation of $F$ can be obtained by analogy with Refs. 57–59, where investigations were reported of higher harmonics of incommensurate magnetic structures induced by an external field or by uniaxial anisotropy. In the temperature range $T_3 < T \leqslant T_2$ this solution is of the form[73]:

$$\psi_x^0(x) = e^{iq_1 x}\Phi_x^0(x), \qquad \Psi_y^0(x) = e^{-iq_2 x}\Phi_y^0(x),$$
$$\Phi_\alpha^0(x) = \sum_{m=-N}^{N} \varphi_\alpha^{(m)} \exp[-2mi(q_1 + q_2)x], \quad (2.9)$$

where the amplitudes of the harmonics $\varphi_\alpha^{(m)}$, as well as the wave vectors $q_1$ and $q_2$, are found by minimization of $F$:

$$\varphi_x^{(1)} = -\frac{4b\varphi_y^{(0)2}\varphi_x^{(0)*}}{a_{xx}(2Q_2 - Q_1)}, \quad \ldots, \quad \varphi_x^{(m)} \sim \varphi_y^{(0)2}\varphi_x^{(m-1)*},$$
$$q_1 = q_1^0 - (q_1^0 - q_2^0)\frac{2|\varphi_x^{(1)}|^2 + 4|\varphi_y^{(1)}|^2}{|\varphi_x^{(0)}|^2} - \ldots. \quad (2.10)$$

Similar expressions for $\varphi_y^{(m)}$ and $q_2$ are obtained after replacement of the subscripts $x, y$ and 1, 2 in Eq. (2.10) with $y, x$ and 2, 1, respectively. Cooling reduces the values of the wave vectors $q_1$ and $q_2$, as indeed confirmed experimentally,[2] and the rate of reduction increases if the dipole forces increase. Figure 2 shows the phase and amplitude of a longitudinal wave $\Phi_x^0(x)$ in the case when $\delta_1 \equiv q_1/q_1^0 = 0.5$. The dependence of the phase on the spatial coordinate $x$ can be described by a step function and is similar to the dependences reported for other physical systems.[60–65] Domain walls (solitons) are then due to a change in the phase and in the amplitude. In the region of domain walls the amplitude decreases following a small peak. Within the domains themselves the state is practically commensurate. The wave period, governed by the distance between the domain walls, is $\pi/(q_1 + q_2)$. A similar soliton form is exhibited by the phase and amplitude of the transverse wave $\Phi_y(x)$.

We shall consider the temperature dependence of the collective modes for two different incommensurate states. Since near the phase transition point the modulus of the vector of the local magnetic moment is not conserved, the dynamic properties of the system are governed not only by precession, but also by vibrational motion.[80,81] The contribution of the latter type of motion may give rise to new branches in the collective mode spectrum (the case of a homogeneous antiferromagnetic resonance is discussed in Refs. 80 and 81 and helical structures are considered in Ref. 66). The vibrational and precession parts of the kinetic energy $K$ are described by terms which are, respectively, quadratic and linear in terms of $\dot{\xi}_\alpha$ (Ref. 81), where $\xi_\alpha(\mathbf{R},t) = \psi_\alpha(\mathbf{R},t) - \psi_\alpha^0(\mathbf{R})$ represents small deviations from the equilibrium states, which are dependent on the spatial coordinates and time. However, in the limit of strong anisotropy, the precession is suppressed.[66] Therefore, it is clear that the precession should be suppressed also in $RbFeCl_3$ because of the planar configuration of the spins ($XY$-like spins), so that the behavior of the collective modes is governed by the vibrational motion and the kinetic energy of such motion is given simply by

$$K = \mu \int d\mathbf{R}\,(|\dot{\xi}_x|^2 + |\dot{\xi}_y|^2),$$

where $\mu$ is the effective mass of fluctuations in the case of such vibrations. The dynamic behavior of the quantities $\xi_\alpha$ is described by complex-conjugate equations

$$\frac{d}{dt}\frac{\delta L}{\delta \dot{\xi}_\alpha^*} - \frac{\delta L}{\delta \xi_\alpha^*} = 0, \quad (2.11)$$

where $L = K - F$ is the Lagrange function.

In the temperature interval $T_2 < T < T_1$, where the incommensurate structure is described by just one component [$\psi_x^0(x) = \varphi_0 \exp(iq_1^0 x)$] different from zero, the Lagrange equations (2.11) are[73]:

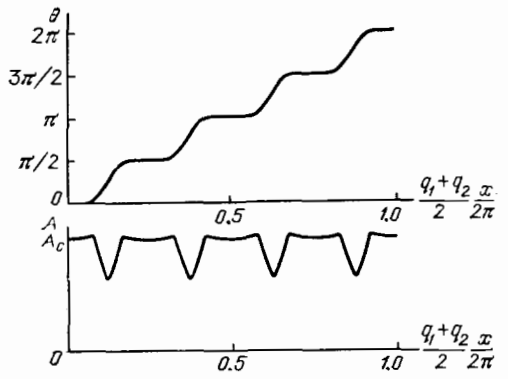


FIG. 2. Spatial dependences of the phase and amplitude of a longitudinal modulation wave $\Phi_x^0(x) = A(x)\exp[i\theta(x)]$ when $\delta_1 \equiv q_1/q_1^0 = 0.5$ ($A_C$ is the amplitude corresponding to a commensurate 120° state).

$$\mu\dot{\xi}_\alpha + \sum_\beta a_{\alpha\beta}(\mathbf{Q}_k - i\nabla)\xi_\beta + 4b(3 - 2\delta_{y\alpha})\varphi_0^2 e^{2iq_1^0 x}\xi_\alpha^* + 8b(3 - 2\delta_{y\alpha})|\varphi_0|^2\xi_\alpha = 0. \quad (2.12)$$

The system (2.12) contains a periodic coefficient in front of $\xi_\alpha^*$ [or in front of $\xi_\alpha$ in the second pair of equations, which are complex conjugate to Eq. (2.12)], which however disappears if we use the transformation $\xi_\alpha \to \xi_\alpha \exp(iq_1^0 x)$. Introducing the Fourier components $\xi_\alpha(\mathbf{k},\omega)$ in equations of the (2.12) type, we find that the expressions for the four eigenfrequencies at $k_y = 0$ are found easily and this corresponds to vanishing also of the off-diagonal components $a_{xy}$ in Eq. (2.12). It follows that the equations for the longitudinal $\xi_x$, $\xi_x^*$ and transverse $\xi_y$, $\xi_y^*$ components of the fluctuations become decoupled.

The spectrum of the collective modes for purely sinusoidal states $\psi_x^0(x)$ is shown in Fig. 3a. The frequency spectrum $\omega(\mathbf{k})$, where $\mathbf{k} = \mathbf{Q} - (\mathbf{Q}_k + \mathbf{q}_1^0)$, does not have discontinuities. In view of the invariance relative to an arbitrary change in the initial phase in $\psi_x^0(x) = |\varphi_0|\exp(iq_1^0 x + \alpha)$ the excitation of one of the branches of the longitudinal components ($\omega_{x-}^2$) in the vicinity of $k_x = 0$ is a phason: At the point $k_x = 0$ the frequency of the branch $\omega_{x-}^2$ vanishes (Goldstone mode) throughout the temperature range where an equilibrium state with the longitudinal modulation wave $\psi_x^0(x)$ can exist. The frequencies of the other branch ($\omega_{x+}^2$) increase as a result of cooling (amplitudon mode—see Refs. 67 and 68). An increase in $k_x$ causes the two branches to intersect a phase (soft) mode $\omega_{y-}^2$ of the transverse components $\xi_y$ and $\xi_y^*$. At the point $k_x = q_1^0 + q_2^0$ (i.e., when $Q_x = Q_k - q_2^0$ in the initial system of coordinates) the soft mode becomes unstable at $T = T_2$: in this case there is additional compensation of the transverse modulation wave $\psi_y^0(x)$.

In a new state with a double incommensurate structure the mode spectrum is of the band type and it has discontinuities at the wave vectors $k_x = n(q_1 + q_2)$; this spectrum is obtained because an unavoidable periodic coefficient now occurs in the transformed Lagrange equations (2.11), i.e., in the equations[73] where the substitutions $\xi_x \to \xi_x e^{iq_1 x}$, $\xi_y \to \xi_y e^{-iq_2 x}$ are made. This situation resembles systems in which modulation of a homogeneous state appears because of the competition between the exchange interactions. In systems of this kind the mode spectrum is also of the band type but only for one of the two main modulated structures which is a simple helix and exhibits a longitudinal spin wave (LSW), namely for the last LSW structure of Ref. 66, where however—in contrast to the structures considered here—discontinuities in the spectrum are due to the single-ion anisotropy.

The spectral pattern of a double incommensurate structure is shown in Fig. 3b using the extended Brillouin zone scheme. In view of the invariance of the changes in the initial phases, the dispersion curves for both components of the order parameter now contain two Goldstone modes. A numerical investigation of the spectrum of the collective modes carried out using finite-difference relationships for the coefficients in the Bloch function[66] shows that a reduction in $\delta_1 = q_1/q_1^0$ and $\delta_2 = q_2/q_2^0$ increases greatly the discontinuities at the edges of the first Brillouin zone; also within the first zone at $\delta_1 \approx \delta_2 = 0.65$ the frequencies of the two lower modes approach zero throughout the interval $0 \leqslant k_x < q_1 + q_2$, which is due to a reduction in the interaction between solitons as a result of an increase in the distance. These modes represent vibrations of domain walls; they are analogous to the modes of a zero-gap branch in the case of systems investigated earlier.[64,65] The upper modes in the first Brillouin zone correspond to vibrations of the thickness of domain walls.

The frequency spectrum of $RbFeCl_3$ was first described in Ref. 82. The neutron scattering measurements reported for the intermediate phases were in qualitative agreement with those calculated and plotted in Fig. 3.

### 2.3. External-field-induced sinusoidal phases in $RbFeCl_3$-type compounds ($CsNiF_3$, $CsFeCl_3$, $CsCuCl_3$)

A magnetic field **H**, applied in the plane of the triangular lattice, deforms the surface of the eigenvalues $\lambda_\pm(\mathbf{Q})$. Depending on the orientation of **H**, the nature of the equipo-

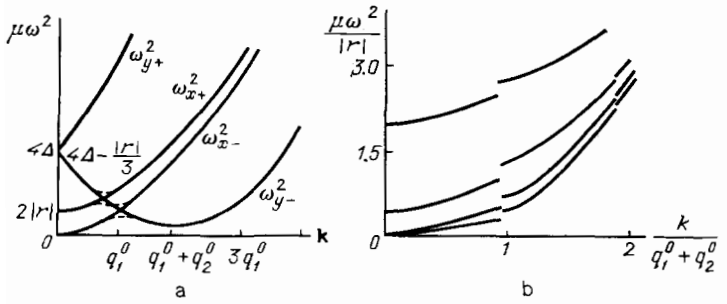


FIG. 3. Spectrum of the collective modes. a) Purely sinusoidal incommensurate structure when only one of the spin components is ordered (the continuous curves represent frequencies with different values of $k_x$ when $k_y = 0$ and the dashed curves correspond to $k_y \neq 0$); $\Delta \equiv \lambda - (\mathbf{Q}_k) - \lambda - (\mathbf{Q}_1) = (\eta\gamma_d)^{2/3}|J_1|$ is the depth of the potential well. b) Double incommensurate structure with simultaneous ordering of both spin components in the case when $\delta_1 \approx \delta_2 = 0.97$.

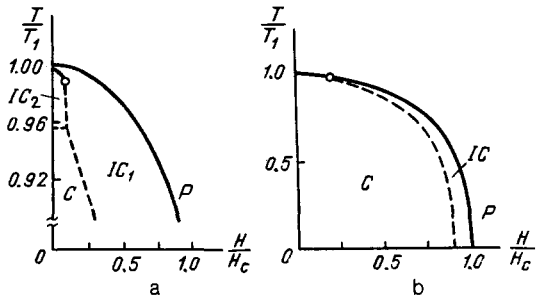


FIG. 4. a) Phase diagram of $RbFeCl_3$ (Ref. 56) when the field is applied along the $y$ axis; the continuous curves represent second-order transitions, whereas the dashed curves correspond to first-order transitions; $C$ is a commensurate state (120° structure), $IC_1$ is an incommensurate state (with a longitudinal modulation wave characterized by $q_1$), $IC_2$ is a double incommensurate structure (with longitudinal and transverse modulation waves characterized by $q_1$ and $q_2$, respectively), $P$ is the paramagnetic phase. b) Phase diagram of $CsNiF_3$ (Ref. 4) (with the field **H** parallel to the $x$ axis); $C$ is a commensurate state with an antiparallel distribution of the spins; $IC$ is an incommensurate state with a modulation wave vector $q_2$.

tential lines shown in Fig. 1c changes in such a way that any state with the point **q** on the dashed contour becomes stabilized.[56] For a fixed direction of the field, the stabilization of a given point is governed by the spin polarization, which rotates smoothly in the case of displacement along the dashed contour. Therefore, if **H** is parallel to the $y$ axis, a state with $\mathbf{q}_1$ becomes stabilized and, vice versa, when the field orientation is parallel to the $x$ axis, the state with $\mathbf{q}_2$ becomes preferable. In finite fields the states with $\mathbf{q}_1$ and $\mathbf{q}_2$ are in the form of a fan structure, because (in addition to sinusoidal waves) the constant component of the magnetization is also induced. If $H$ is sufficiently high, a modulated state is possible also at $T = 0$. Figure 4a shows the phase diagram of $RbFeCl_3$ for a magnetic field applied along the $y$ axis[56]; the line of transitions between different incommensurate phases includes a tricritical point. The $T$–$H$ phase diagram is in qualitative agreement with the experimental data[2]: the fan structure is observed in strong fields, whereas the double incommensurate structure is observed only in weak fields.

In the case of the hexagonal magnetic compound $CsNiF_3$ (which is isomorphous with $RbFeCl_3$) the experimentally detected[69] ground state is a structure with an antiparallel orientation of the spins in the basal plane (one of the three equivalent states with $\mathbf{Q}_M$ is shown in Fig. 5a). An important role in the formation of this structure is played by the dipole interaction,[70] because in the case of $CsNiF_3$ the value of $\gamma_d$ is of the same order as $J_1$. Cooling induces a transition from the paramagnetic state to a state with $\mathbf{Q}_M$ which is realized in this compound immediately without the formation of an intermediate incommensurate phase. However, in an external field **H**, oriented along the $x$ axis, a modulated phase may appear and it has a wave vector $\mathbf{Q}_2$. The change in the spin structure on increase in $H$ is shown in Fig. 5b for the case when $T = 0$. In fields lower than $H_{IC}$ there is a two-sublattice state with a nonzero component of the spin not only along the $x$ axis, but also along the $y$ axis; when a field reaches the critical value $H_{IC}$, a transition to a fan structure involves an abrupt change in the homogeneous magnetization. At finite temperatures the phase diagram has the form shown in Fig. 4b.

The ground state of another isomorphous crystal $CsFeCl_3$ differs from that of $RbFeCl_3$ because it is nonmagnetic since the single-anisotropy represented by the parameter $D = 15.8$ K (Ref. 71) is larger than the intrachain ferromagnetic coupling constant $J_0 = 7.4$ K (Ref. 71); in this case the interchain antiferromagnetic coupling constant is $J_1 = -1.8$ K. Neutron diffraction studies of this crystal have demonstrated that in an external field parallel to the $c$ axis there are Bragg peaks at $T = 0.7$ K if $H > 3.8$ $T$. In fields above such critical values there are incommensurate phases (analogous to the phases reported in Ref. 2 for $RbFeCl_3$ in $H = 0$) with their wave vectors **Q** close to the high-symmetry point $K$. Cooling destroys the satellites near the high-symmetry point $K$ and a 120° structure appears in the magnetic field. These effects can be explained[72] allowing for the correlation effects leading to a situation that in a field applied along the $c$ axis the conical high-symmetry point becomes unstable. In the random-phase approximation the results of calculations of the critical fields[72] are in good agreement with the experimental data.[5]

X-ray and neutron diffraction investigations demonstrate clearly that the hexagonal crystals of $CsCuCl_3$ undergo a structural phase transition[74–77] associated with a helicoidal displacement of the $Cu^{2+}$ ions at 423 K. Below the transition point from the paramagnetic phase (10.7 K) the antiferromagnetic interaction between the chains in $CsCuCl_3$ induces a triangular (120°) magnetic structure in the basal plane and a strong exchange coupling within the chains, together with a weak anisotropy described by the Dzyaloshinskiĭ interaction, gives rise to a helical structure modulated along the $c$ axis.[78] Therefore, in contrast to $RbFeCl_3$, this particular magnetic crystal has no sinusoidal structure because it is suppressed by the dipole mechanism.

For arbitrary relationships between the dipole and the Dzyaloshinskiĭ interactions, the latter described by

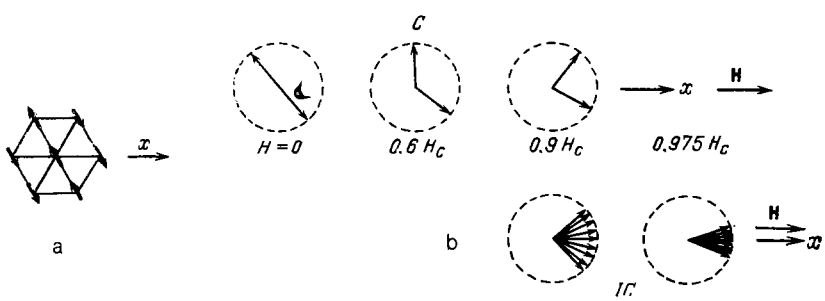


FIG. 5. Spin structures of incommensurate and commensurate states of $CsNiF_3$ (Ref. 4): a) ground state in zero field; b) states in different fields **H** along the $x$ axis ($T = 0$).

$$\mathcal{H}_D = \sum_{i,j} D_{ij}^z [\mathbf{S}_i \times \mathbf{S}_j]_z \qquad (2.13)$$

(because of the crystal symmetry the vector $\mathbf{D}_{ij}$ has only one component $D_{ij}^z$), the presence of a given structure which appears at an instability point $T_1$ of the symmetric phase depends on the relationship between the intrachain and interchain exchange constants $J_0$ and $J_1$. The eigenvalues of the Fourier components of the total Hamiltonian have the following form in the approximation quadratic in $\mathbf{q} = \mathbf{Q} - \mathbf{Q}_k$ (Ref. 78) (it is assumed here that the constants $a$ and $c$ amount to unity):

$$\lambda_{\pm}(\mathbf{q}) = C + J_0 q_z^2 + \frac{3}{4} J_1 q_\perp^2 \pm [(\eta\gamma_d q_\perp)^2 + (2Dq_z)^2]^{1/2}, \qquad (2.14)$$

where $C$ is a constant which depends on the exchange parameters $J_0$, $J_1$, and $\gamma_d$; $D = |D_{i,i\pm1}^z|$. Hence, it is clear that if $D = 0$, a minimum of the function $\lambda_-(\mathbf{q})$ occurs on a circle $q_1^2 \equiv q_x^2 + q_y^2 = (2\eta\gamma_d/3J_1)^2$, where $q_z = 0$. An allowance for the terms which are cubic in $\mathbf{q}$ in Eq. (2.2) for $J(\mathbf{Q})$ lifts the continuous degeneracy of $\lambda_-$ around $\mathbf{Q}_k$, so that—as expected—there are three equivalent points $\mathbf{q}_1$ shown in Fig. 1b. Conversely, if $\gamma_d = 0$, then a minimum of $\lambda_-(\mathbf{q})$ is obtained when $q_z = D/J_0, q_\perp = 0$. Figure 6a shows the range of existence of various phases which appear below the transition point $T_1$. For a fixed value of $J_0 / |J_1|$ a specific spin configuration is formed and the nature of this configuration depends on the ratio $D/\eta\gamma_d$. If the inequality [57]

$$\frac{D}{\eta\gamma_d} > \left(\frac{J_0}{3|J_1|}\right)^{1/2} \qquad (2.15)$$

is satisfied, a sinusoidal wave in the basal plane does not condense: instead, a helix with a modulation period along the $c$ axis is observed. The condition (2.15) is obeyed well by a crystal of $CsCuCl_3$, since according to the experimental data reported in Refs. 77 and 79 this compound is characterized by $J_0/|J_1| \approx 8$, $D/\eta\gamma_d \approx 20$.

In the case of those compounds which satisfy the inequality (2.15), a helical structure may not appear at all in a magnetic field.[6] At values of $H$ above the critical the field induces an unstable conical high-symmetry point, which is manifested by a shift of the curve in Fig. 6a in the direction of the helical phase. Consequently, the existence of a sinusoidal wave with a modulation period on a triangular lattice becomes possible below the temperature of the transition from the paramagnetic phase. The critical value of the field in the basal plane is then

$$H_c = 2|J_1| \left\{ \frac{1}{J_0} \left[ \frac{D^2}{J_0} - \frac{(\eta\gamma_d)^2}{|3J_1|} \right] \right\}^{1/2}. \qquad (2.16)$$

Estimates based on Eq. (2.16) obtained for a $CsCuCl_3$ crystal give $H_c \approx 0.3$ T, which is in agreement with the experimental values. However, further cooling makes the sinusoidal state (in an external field $H > H_c$) thermodynamically unstable at the temperature $T = T_2$ below which the free-energy minimum corresponds to the helical phase.[6,78] Therefore, for the compounds satisfying the inequality (2.15) we can expect, depending on temperature, two different incommensurate phases: a helical one with $q_z \neq 0$ and a sinusoidal one with $q_\perp \neq 0$ (Fig. 6b).

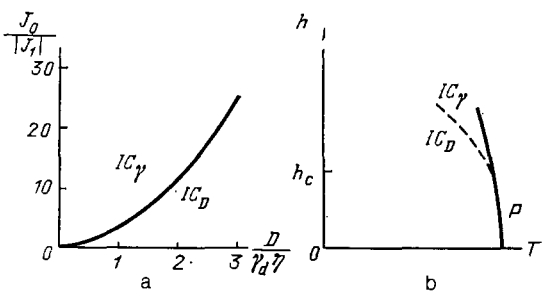


FIG. 6. a) Range of existence of incommensurate phases which appear as a result of instability of the paramagnetic phase of $CsCuCl_3$ ($H = 0$); $IC_\gamma$ is a sinusoidal incommensurate structure in the basal plane and $IC_D$ is a helical structure with a modulation period along the $c$ axis of the hexagonal lattice. b) Phase diagram of the same compound.

## 3. STATES OF THE PLANAR SPIRAL TYPE AND TRIANGULAR SUPERSTRUCTURES

### 3.1. Helical configurations in transition-metal halides and in compounds similar to the β phase of solid oxygen

In some transition-metal compounds, such as the rhombohedral antiferromagnet $NiBr_2$ (with the space group $D_{3d}^5$), thermal fluctuations induce a transition of a helical structure to a commensurate intermediate state.[9-13] Resonance measurements have established[11] that such centrosymmetric compounds exhibit a modulated structure as a result of competition between the exchange interactions of different signs. Villain[14] used the example of classical planar spins on a square lattice to demonstrate the importance, in the temperature-induced changes of the wave vector, of the structure of the thermal renormalization exchange constants due to the interaction between spin waves. Such renormalizations occur even in the self-consistent harmonic approximation with a temperature-dependent effective Hamiltonian. In the case of the $XY$ spins this approximation is equivalent to a variational procedure[88] applied to the problem of a nonlinear response of a two-dimensional isotropic nematic; the results reported in Ref. 88 agree or are close to more rigorous results by Berezinskiĭ[26] obtained for the same physical problem.

In the case of easy-plane magnetic materials we can expect quantum fluctuations to reduce further the wave vector of the modes. Therefore, in contrast to classical planar spins[14] (and similar systems[88]) it is necessary to write down the temperature-dependent harmonic Hamiltonian in terms of two (canonical) variables $\theta_i$ and $s_i^z$ which represent the generalized coordinates and momenta[89,90]:

$$\mathcal{H} = \sum_{\mathbf{k}} (a_{\mathbf{k}} |\theta_{\mathbf{k}}|^2 + b_{\mathbf{k}} |s_{\mathbf{k}}^z|^2). \qquad (3.1)$$

The fluctuating quantities $\theta_i$ and $s_i^z$ represent small deviations at a site $i$ of, respectively, the azimuthal angle $\varphi_i$ of the spin which deviates from the thermodynamic-equilibrium values of the phases of the helix $\mathbf{Q}\cdot\mathbf{R}_i$ and of the spin projection $S_i^z$ which deviates from the constant component of the spin $m$ along the field applied parallel to the $c$ axis, i.e., $\theta_i = \varphi_i - \mathbf{QR}_i$, $s_i^z = S_i^z - m$; $a_{\mathbf{k}}$ and $b_{\mathbf{k}}$ are the variational parameters.

The wave vector of the helix $\mathbf{Q}$, the constant component of its spin $m$, and the parameters $a_{\mathbf{k}}$ and $b_{\mathbf{k}}$ are found from a system of equations obtained as a result of minimization of

the free energy[15] carried out using the test Hamiltonian of Eq. (3.1):

$$\sum_{i-j} \tilde{J}_{ij}\mathbf{R}_{ij} \sin(\mathbf{Q}\mathbf{R}_{ij}) = 0, \quad m = \frac{1}{2}\frac{H}{D + \tilde{J}_0^s - J_0},$$
$$a_k = (\tilde{J}_0^s - \tilde{J}_k^s)\left(S^2 - m^2 - N^{-1}\sum_{k'}\langle|s_{k'}^z|^2\rangle\right), \qquad (3.2)$$
$$b_k = \tilde{J}_0^s - J_k + D, \quad \tilde{J}_k^s = \frac{1}{2}(\tilde{J}_{Q+k} + \tilde{J}_{Q-k});$$

here, $D$ is the anisotropy constant of the easy-plane type ($D>0$); $N$ is the number of spins; $\tilde{J}_k = \Sigma_{i-j}\tilde{J}_{ij}\exp(i\mathbf{k}\mathbf{R}_{ij})$ are the Fourier components of the exchange constants renormalized by thermal fluctuations:

$$\tilde{J}_{ij} = J_{ij}\exp\left[-N^{-1}\sum_k \langle|\theta_k|^2\rangle(1 - e^{i\mathbf{k}\mathbf{R}_{ij}})\right]. \qquad (3.3)$$

The correlation functions of the fluctuating quantities in Eqs. (3.2) and (3.3) are obtained allowing for the zero-point vibrations as follows:

$$\langle|\theta_k|^2\rangle = \frac{\omega_k}{4a_k}\operatorname{cth}\frac{\omega_k}{2T}, \quad \langle|s_k^z|^2\rangle = \frac{\omega_k}{4b_k}\operatorname{cth}\frac{\omega_k}{2T} \qquad (3.4)$$

[$\omega_k = 2(a_k b_k)^{1/2}$ is the spectrum of spin waves].

In the case of $NiBr_2$-type compounds the exchange integral for the nearest spins $J_1$ on a triangular lattice is positive, whereas for the second- and third-nearest neighbors the exchange integrals $J_2$ and $J_3$ are negative (Fig. 7a). Moreover, the exchange integral for the nearest spins in the neighboring layers of the rhombohedral lattice is also negative ($J'<0$). Since the triangular lattice plane in $NiBr_2$ coincides with the easy magnetization plane, in systems of this kind the wave vector of the helix is in the plane of polarization of the spins (planar spiral state). Figure 7b shows the dependence of $m$ on $T$ for $NiBr_2$: It is similar to the dependence found experimentally.[9] A graph of the dependence of $Q$ on $T$ for two initial values ($T=0$) of $Q_0 = [2(4|J_3| - J_1)/3J_1]^{1/2}$ amounting to 0.07 and 0.1 is plotted in Fig. 7c for $J_2 = 0$. The resultant curves allow for the thermal and quantum fluctuations of both $\theta$ and $s^z$. An increase in $H$ reduces the temperature range of existence of this spiral structure (this follows from a comparison of the lower curves plotted for $Q_0 = 0.07$); this reduction in the temperature range on increase in the field along the $c$ axis is due to an increase in the phase fluctuations because of a reduction in the spin projection in the basal plane. However, an increase in the interplanar interaction increases the range of existence of the incommensurate phase (which in turn follows from a comparison of the upper curves representing the case when $Q_0 = 0.1$). These dependences are in qualitative agreement with the experimental data reported in Refs. 9, 10, and 13. At $T=0$ the renormalization of the exchange integrals in Eq. (3.3) is entirely due to quantum fluctuations: the value $Q = Q_0$ decreases both on increase in $D$ and on increase in $H$. If the wave vector of the helix is sufficiently small, the external field can destroy the helical structure even at $T=0$.

The stability of the incommensurate states depends strongly not only on the dimensions of space, but also on the nature of the lattice (triangular or square) on which spins are distributed in the layers of a crystal, because the spectrum of long-wavelength fluctuations may be very different for the states formed on these different lattices. For example, in the case of layer triangular-lattice systems the long-range order is observed (in contrast to square lattices) along certain directions, whereas along other directions the correlations decrease in accordance with a power law.[15]

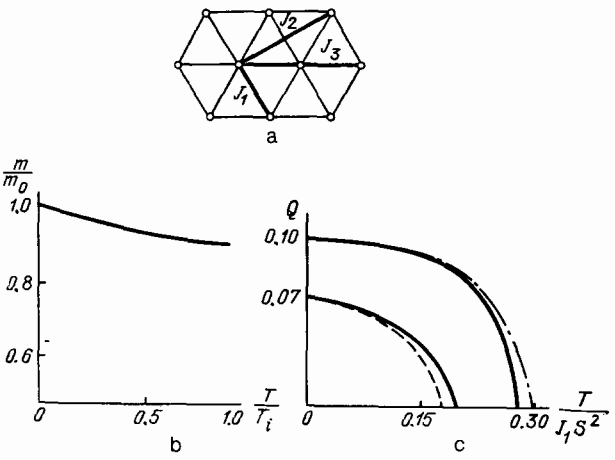


FIG. 7. a) Constants of the exchange interactions between the spins on a triangular lattice. b) Temperature dependence of the magnetization $m$ along the $c$ axis of the rhombohedral lattice (weak fields); $J_3/J_1 = -0.255$, $J'/J_1 = -0.1$, $D/J_1$ 0.05. c) Temperature dependences of the wave vector of a planar spiral ($D/J_1 = 0.05$); the continuous curves apply to the field $H=0$ when $J'/J_1 = -0.1$, whereas the dashed curve corresponds to $H/J_1S = 0.01$ and $J'/J_1 = -0.1$, and the chain curve corresponds to $H=0$ and $J'/J_1 = -0.15$.

The competition between the exchange interactions in a rhombohedral crystal can in this case be solely due to the presence of a coupling between the nearest spins: the coupling is antiferromagnetic $J_1$ ($<0$) in the basal plane and interplanar $J'$ (of any sign). For $0<|J'|<3|J_1|$, the state with the minimum energy is a helical configuration of spins. Moreover, the ground-state energy is continuously degenerate relative to the wave vector $\mathbf{Q}_*$ of inequivalent helices differing from one another in respect of the orientation and of the value of $Q_*$ itself. If $|J'| \ll 3|J_1|$, the equipotential lines of the degenerate states represent turns on the surfaces of six cylinders. In the three-dimensional $\mathbf{Q}$ space these cylinders have identical radii $2|j'|/\sqrt{3}a$, where $j' = J'/J_1$, and the same heights $6\pi/c$; the axes of these cylinders are parallel to the $c$ axis. These axes intersect with the $Q_x, Q_y$ plane (the coordinate axes are oriented so that $Q_y$ is parallel to the translation vector $a$ of the triangular lattice) at six equivalent sites $(0, \pm 4\pi/3a)$, $(\pm 2\pi/\sqrt{3}a, \pm 2\pi/3a)$. Near one of them $(0, 4\pi/3a)$ the equations for the degenerate values of $Q_*$ are[48]

$$Q_*^x = -\frac{2j'}{\sqrt{3}a}\sin\frac{cQ_*^z}{3},$$
$$Q_*^y = \frac{4\pi}{3a} + \frac{2j'}{\sqrt{3}a}\cos\frac{cQ_*^z}{3}, \qquad (3.5)$$
$$-\frac{3\pi}{c} < Q_*^z < \frac{3\pi}{c}.$$

If $j' = 0$, the ground state reduces to a 120° structure without any dependence on the spin orientations between the different layers. However, in the case of even infinitesimally small but finite values of $j'$, we find that $\mathbf{Q}_*$ is degenerate and a phase dependence is observed for neighboring layers. If $|j'| \to 1$, the cylinders transform continuously into prisms with a triangular base (projections of the lines of degeneracy on the $Q_x, Q_y$ plane are plotted in Fig. 8 for different values of $j'$). When the values of $j'$ lie within the range $1 < |j'| < 3$,

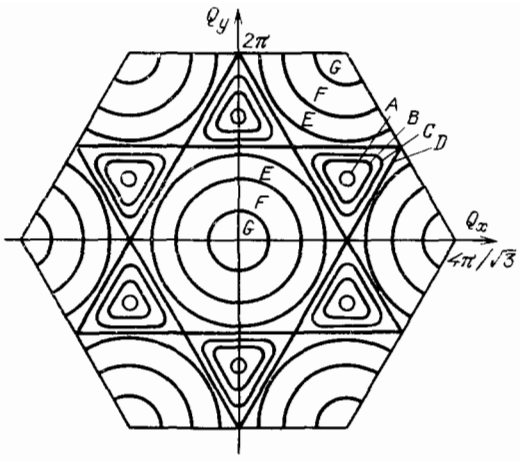


FIG. 8. Projection of the lines of degeneracy onto the $Q_x$, $Q_y$ plane plotted for different values of $j'$ (Ref. 48): A) $j' = 0.15$; B) $j' = 0.5$; C) $j' = 0.8$; D) $j' = 1$; E) $j' = 1.2$; F) $j' = 2$; G) $J' = 2.8$.

the equipotential lines consist of seven parts. In the limit $|j'| \to 3$ the radii and heights of the cylinders (of the central one and of the six other cylinders consisting of one-third of the cylindrical surface) tend to zero since for $|j'| = 3$ we can expect a homogeneous state corresponding to the point $Q_*^x = Q_*^y = 0$, as well as six other points equivalent to the first one. However, the value of $Q_*^z$ depends on the sign of $j'$: if $j' = -3$, then $Q_*^z = 0$, and conversely if $j' = 3$, then $Q_*^z = 3\pi/c$.

It is interesting to note that the projections of the lines of degeneracy on the $Q_x$, $Q_y$ plane resemble a pattern of the distribution of the effective exchange field created by ions with the reversed spins in the "mixed" state, observed in strong magnetic fields, of antiferromagnetic $FeCO_3$, as reported by Dudko *et al.*[83] Moreover, they resemble also the lines of force of incommensurate structures in dipole systems with a weak exchange interaction.[43]

In the absence of anisotropy the spin-wave spectrum contains a soft mode for all the values of $\mathbf{Q}_*$ along a line of degeneracy. The presence of a "soft line" destroys the long-range order at any finite temperature.[48] However, it is found that an allowance for the zero-point vibrations lifts the continuous degeneracy of the ground state relative to $\mathbf{Q}_*$ and leaves only a discrete state.[49] Therefore, even in the isotropic case the quantum effects restore the long-range order. Nevertheless, at sufficiently high temperatures when the quantum fluctuations are unimportant, the state of the system is similar to the state with "degenerate helices." In fact, recent calculations[37] demonstrate that quantum fluctuations induce a phase transition in systems of this kind; a state with inequivalent helices then appears in the intermediate phase.

An example of a rhombohedral system which can manifest these properties is the $\beta$ phase of solid oxygen.[84,84] An analysis of thermal and magnetic properties of this compound led Loktev[86] to put for the first time the hypothesis that the magnetic structure of $\beta$–$O_2$ represents a three-sublattice noncollinear (canted) antiferromagnet. The $\beta$ phase of oxygen represents a molecular crystal which is a planar ($XY$) magnetic material with the dominant antiferromagnetic coupling $J_1$ between the $O_2$ molecules in the basal plane and a weak coupling $J'$ between the planes.[50] Neutron scattering experiments carried out on polycrystalline samples[91,92] revealed a wide peak in the vicinity of the high-symmetry point $\mathbf{Q}_k$ corresponding to a 120° structure. The width of this peak is independent of temperature, and it follows, as demonstrated by the calculations in Ref. 48, that it is governed by the minimum and maximum values of $\mathbf{Q}_*$ for "degenerate helices." The limits of the temperature of the transition to a state with a fixed wave vector of the helix, i.e., to a state where quantum fluctuations are important, shows that in the case of $\beta$ oxygen we have $T_c = 14$ K (Ref. 37). However, at this temperature the rhombohedral lattice of the $\beta$ phase is unstable: Instead a monoclinic lattice ($\alpha$ phase) is observed between 0 and 24 K.

### 3.2. Triangular domain superstructures. Partly disordered states in $CsCoCl_3$ and $CsCoBr_3$

In this subsection we shall consider Ising spin systems with triangular lattices. We shall first assume that a triangular lattice is formed by chains (it is hexagonal) and the interaction within the chains is ferromagnetic ($J_0 > 0$). In an external field the ground state with nonzero exchange constants $J_1$ and $J_2$ ($J_3 = 0$) was reported in Refs. 93 and 94. In the case of frustrated Ising systems when the antiferromagnetic coupling ($J_1 < 0$) is established between the nearest spins on a triangular lattice and the second-nearest spins are characterized by $J_2 \gtrless 0$, the phase diagram is of the kind shown in Fig. 9. At zero temperature, depending on $h = H/|J_1|$ and $\alpha = J_2/J_1$, we can expect six different phases with the unit cells (and their designations) shown in Fig. 9; two configurations ($3\times3$ and $3\times1$) are energy-degenerate: the degeneracy is lifted if we assume that, for example, $J_3 \neq 0$.

At an interface between the $3\times3$ and $2\times2$ phases, where the condition $H = 2J_1 - 6J_2$ is satisfied, we can find a domain wall within which the energy vanishes. In the presence of a domain wall within the $3\times3$ structure the energy of its formation (per unit length) is[51]:

$$E_{DB} = \frac{2}{9}(-H + 2J_1 - 6J_2). \tag{3.6}$$

The continuous lines in Fig. 10a represent the only domain walls which have zero energy at the interface between the $3\times3$ and $2\times2$ phases. This periodic distribution of the walls gives rise to commensurate higher-order structures in such a

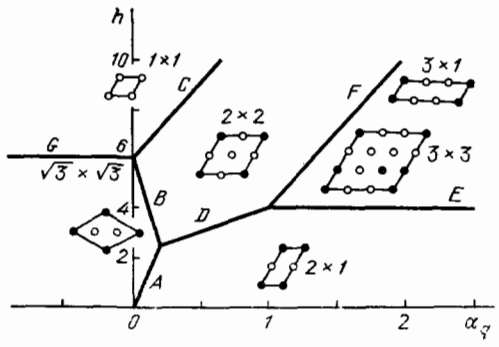


FIG. 9. Phase diagram at temperatures close to absolute zero, showing the Ising spins on a triangular lattice ($h = H/|J_1|$, $\alpha = J_2/J_1$). The unit cells of the spin structures for each of the phases in the ground state are shown directly in the figure; the open circles and the black dots represent $S = 1$ and $S = -1$, respectively. The $3\times1$ and $3\times3$ phases are energy-degenerate.[94,103]

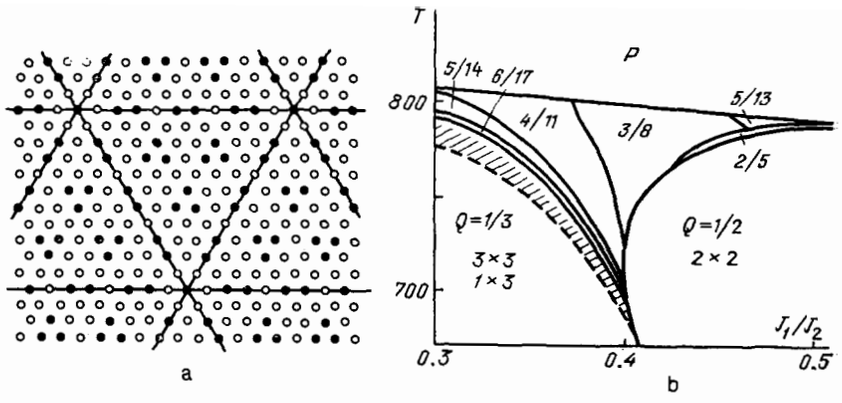


FIG. 10. a) Triangular domain superstructure with $Q = 4/11$; the domain walls are represented by continuous lines. b) Phase diagram for $J_0 = 1717$ K, $H = 23.5$ K, and $J_1 + J_2 = -0.275H$ (Ref. 51). Here, $T$ is in kelvin.

way that they form a triangular domain superstructure. Figure 10a represents a long-period structure with $Q = 4/11$ (4/11 structure) for which the largest value of the Fourier component (with the exception of the constant contribution) is localized at $\pm Q\mathbf{K}_s$ with $Q = 4/11$, where $\mathbf{K}_s$ is the reciprocal lattice vector; we can see from the figure that the $2\times2$ structure is realized partly near the points of intersection of the domain walls. In general, different triangular superstructures can form with $Q = n/(3n-1)$, where $n = 1, 2, 3, \ldots$. In terms of this notation the $2\times2$ structure is characterized by $Q = 1/2$ $(n = 1)$ and the $3\times3$ structure by $Q = 1/3$ $(n = \infty)$. The energy of such states per one site is

$$E(n) = E(\infty) + \frac{3(3n-2)}{(3n-1)^2} E_{DB}, \tag{3.7}$$

where $E(\infty) = -J_0 - (H + J_1 - 3J_2)/3$ is the energy of the $3\times3$ structure. All the spin configurations characterized by $Q = n/(3n-1)$ are degenerate when $H = 2J_1 - 6J_2$ $(E_{DB} = 0)$. We note that the additional energy due to the intersection of domain walls also vanishes in fields $H$ which correspond to the interface between the $2\times2$ and $3\times3$ phases.

If $T \neq 0$, we can expect triangular superstructures to be stabilized by an increase in entropy. If, moreover, directly below the transition point of a paramagnetic phase the stable structures are described by the wave vector $\pm Q\mathbf{K}_s$ with $\cos 2\pi Q = -(J_1 + J_2)/2J_2$, i.e., if $Q$ corresponds to the maximum value of the Fourier component of the exchange interactions $J(Q)$, we can expect such modulated states to become stabilized in a wide range of temperatures.

Minimization of the free energy

$$F = -\sum_{\mathbf{R},\mathbf{R}'} J(\mathbf{R},\mathbf{R}')\langle S(\mathbf{R})\rangle\langle S(\mathbf{R}')\rangle - H\sum_{\mathbf{R}}\langle S(\mathbf{R})\rangle + T\sum_{\mathbf{R}}\int_0^{\langle S(\mathbf{R})\rangle} M^{-1}(x)\,dx, \tag{3.8}$$

written down allowing exactly for the intrachain interaction (on the assumption that $|J_0| \gg |J_1|, |J_2|$) where $M^{-1}$ is the inverse function of

$$M(x) = \operatorname{sh} x \cdot [\exp(-2|J_0|T^{-1}) + \operatorname{sh}^2(x)]^{-1/2}, \tag{3.9}$$

has been carried out for the structures with $Q = n/(3n-1)$ and for those with $Q = m/l$ ($n$, $m$, and $l$ are integers). Figure 10b shows the phase diagram obtained as a result of numerical calculations ($n = 1, 2, \ldots, 7$ and $\infty$; $m < l \leqslant 14$); in the shaded region there are structures with $Q = n/(3n-1)$ characterized by $n \geqslant 8$. The dashed line in the same figure corresponds to zero of the free energy of domain walls. At $T \neq 0$ the $3\times3$ structure is still degenerate with the $3\times1$ structure. The state with $Q = 5/13$ is observed at sufficiently high temperatures. This is due to the fact that this state does not belong to the class of degenerate states characterized by $Q = n/(3n-1)$. Naturally, other structures not considered in numerical calculations can also appear. However, their existence is for these reasons possible only at high temperatures.

Near the critical point an analysis of the structures carried out on the basis of the free energy written in the form of the Ginzburg–Landau expansion shows that if $Q \approx 1/3$, we still have a lattice of domain walls where the $3\times3$ structure is obtained.

Equation (3.8) can explain, for example, the main mechanism responsible for the existence of a modulated structure in such a compound as superionic conductor $\beta$-$LiAlSiO_4$. This compound has a hexagonal lattice and the sites in this lattice may be occupied by Li. Neutron-diffraction experiments[95,96] have shown that in the case of Al and Si layers alternating along the $c$ axis the ratio of the probabilities of finding Li in the Al layers differs from the corresponding probability for the Si layers and the two probabilities are in the ratio 1/3. The disordered Li atoms form stable states as a result of cooling. For example, in the commensurate state we can expect the $2\times2$ structure in which every second site on a triangular lattice is occupied by Li and a modulated phase exists in the intermediate range of temperatures $T$. The experimental data for $\beta$-$LiAlSiO_4$ agree with the results obtained for Ising systems. In accordance with the experimental observations, we must postulate here the presence of a field which alternates in sign from one layer to the next, as well as the presence of an intrachain antiferromagnetic coupling. The Hamiltonian corresponding to Eq. (3.8) satisfies these requirements if we make the transformation $S(i,\mathbf{R}) \to (-1)^i S(i,\mathbf{R})$, where $i$ labels the positions of the spins along the $c$ axis. Since, moreover, the interaction between the Li ions is of the Coulomb nature, it is natural to assume that the coupling between the spins in a triangular lattice is antiferromagnetic. If the ratio $J_1/J_2$ is sufficiently large, it follows from Fig. 10b (where the values $J_0 = 1717$ K and $H = 23.5$ K are selected in order to apply the theory to $\beta$-$LiAlSiO_4$), we can expect a transition from the $2\times2$ to a modulated structure on increase in temperature, which is in agreement with the experimental results.

The interaction between the second-nearest neighbors

on a triangular lattice in Ising magnetic materials $CsCoCl_3$ and $CsCoBr_3$ is ferromagnetic ($J_1<0$, $J_2>0$) so that a $\sqrt{3}\times\sqrt{3}$ structure becomes stabilized in the ground state: this structure has three spins in a unit cell (Fig. 9). At finite temperatures such antiferromagnets exhibit[16,17] two phase transitions and in the case of $CsCoCl_3$ they occur at $T_1 = 21.3$ K and $T_2 = 9.2$ K (Ref. 16).

The self-consistent equations for the three magnetic sublattices (Fig. 11a) are

$$\langle S_n\rangle = M(L_n), \tag{3.10}$$

where the arguments $L_n$ of the function $M$ of Eq. (3.9) are given by:

$$L_1 = \frac{3J_1}{2T}(\langle S_2\rangle + \langle S_3\rangle + 2\alpha\langle S_1\rangle),$$

$$L_2 = \frac{3J_1}{2T}(\langle S_3\rangle + \langle S_1\rangle + 2\alpha\langle S_2\rangle),$$

$$L_3 = \frac{3J_1}{2T}(\langle S_1\rangle + \langle S_2\rangle + 2\alpha\langle S_3\rangle)$$

$$(\alpha = J_2/J_1).$$

The system of equations (3.10) predicts a sequence of phase transitions. At low values of $|\alpha|$ there are three ordered phases[97]: partly disordered (PD) characterized by $\langle S_1\rangle = -\langle S_2\rangle \neq 0$, $\langle S_3\rangle = 0$ (Fig. 11b); a three-sublattice ferrimagnetic phase (3FR) characterized by $\langle S_1\rangle$, $\langle S_2\rangle$, $\langle S_3\rangle \neq 0$; a two-sublattice ferrimagnetic phase (2FR) characterized by $\langle S_1\rangle = \langle S_3\rangle > 0$, $\langle S_2\rangle < 0$. Lowering of $T$ gives rise to PD→3FR→2FR transitions. In the case of moderately large values of $|\alpha|$, only the PD and 2FR phases exist and any transition between them is of the first order. Finally, if $|\alpha|$ is large, only one ordered phase 2FR remains.

The paramagnetic state ($P$) is unstable compared with $PD$ or 2FR at the point $T = T_1$, as deduced from the equation[18]

$$\frac{3}{2}\frac{|J_1|}{T}(1-2\alpha)\exp\frac{|J_0|}{T_1} = 1. \tag{3.11}$$

In turn, the partly disordered phase is unstable at $T = T_0$ and we have

$$3\frac{J_2}{T_0}\exp\frac{|J_0|}{T_0} = 1. \tag{3.12}$$

If the 3FR phase is stable, then $T_0 = T_2$ and this is the point of a second-order transition from the PD to the 3FR state. However, if a first-order transition takes place from PD to 2FR at $T = T_2$, then $T_2$ is higher than $T_0$. The phase diagram for arbitrary values of $T_0$ [which correspond to specific values of $J_2$ in Eq. (3.12)] is presented in Fig. 11c. The values $T_1 = 21.3$ K and $J_0 = 75$ K represent $CsCoCl_3$. Assuming also that in the case of $CsCoCl_3$ we have $\alpha \approx -2\times10^{-3}$, we find that the results predict two phase transition points, which is in agreement with the experiments.

A qualitatively similar result was obtained by the cluster variational method in Ref. 19. The Monte Carlo method used in Refs. 20 and 21 predicted that the intermediate phase in $CsCoCl_3$ and $CsCoBr_3$ should be described by $\langle S_j\rangle \propto \cos(\mathbf{Q}_k\cdot\mathbf{R}_j + \alpha)$ with a phase $\alpha = \alpha(\mathbf{R}_j, t)$ varying at random in space and time. The phase $\alpha$ changes little inside a domain, but it varies rapidly in domain walls. A reduction in temperature reduces the fluctuations of the phases, so that only the 2FR phase exists at the transition point. These results can account for the observation, at moderate temperatures, of large fluctuations in time of the magnetic structure of a $CsCoCl_3$ crystal reported in Ref. 16.

## 4. PHASE TRANSITIONS IN TWO-DIMENSIONAL FRUSTRATED ANTIFERROMAGNETS

### 4.1. Phase diagram for Ising spins on a triangular lattice

In two-dimensional Ising antiferromagnets, where the interaction is limited to the nearest neighbors on a triangular lattice, spin ordering is greatly weakened because of the frustration effects. A system of this kind then shows no phase transition at any finite temperature.[98-100] However, an allowance for the interactions of the second-nearest neighbors stabilizes the spin state and the system undergoes a phase transition similar to that expected for the ferromagnetic $XY$ model when the field breaks the sixfold symmetry.[101]

If $H \neq 0$, the transition between the ground states on a triangular lattice may appear because of the formation of a local spin structure in the initial phase and this structure is similar to that in the adjacent phase. Domain walls responsible for the formation of such a local structure can be found along lines $A$, $C$, $D$, $E$, and $G$ (Fig. 9), which separate the adjacent states in the phase diagram. The appearance of such walls in critical fields does not require additional energy. In the case of lines $B$ and $F$ in Fig. 9 such zero-energy walls cannot form because of the specific geometric nature of the spin structures of two adjacent phases.

A phase diagram can be constructed for finite temperatures if the free energy of domain walls $\mathcal{F}$ is calculated by the interphase configuration method.[102] The easiest to find is the line of transitions between the $2\times1$ phase and the paramagnetic phase when the values of $\alpha(=J_2/J_1)$ lie between 0.2 and 1. Since in this interval of $\alpha$ the $2\times1$ adjoins the $2\times2$ phase in the diagram representing the ground states (Fig. 9),

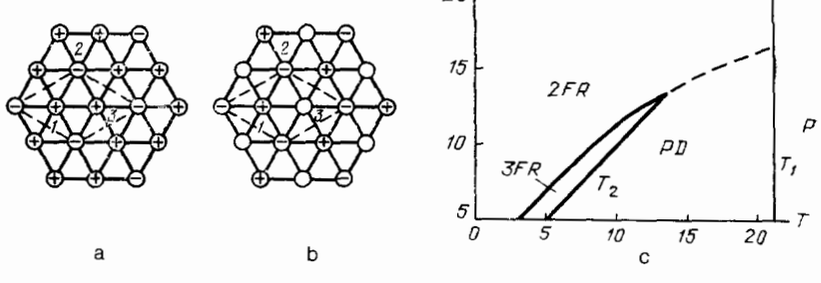


FIG. 11. a), b) Magnetic ordering in $CsCoCl_3$ and $CsCoBr_3$ at temperatures $T<T_1$ (a) and $T_2<T<T_1$ (b); the plus and minus signs represent, respectively, the up and down spin orientations; an empty circle represents a disordered state in the chain. c) Phase diagram. Here, $T_1$ is 21.3 K and it is assumed that $J_0 = 75$ K, which corresponds to the experimental values of $CsCoCl_3$. The dashed curve represents a first-order transition and the continuous curve represents a second-order transition.[18]

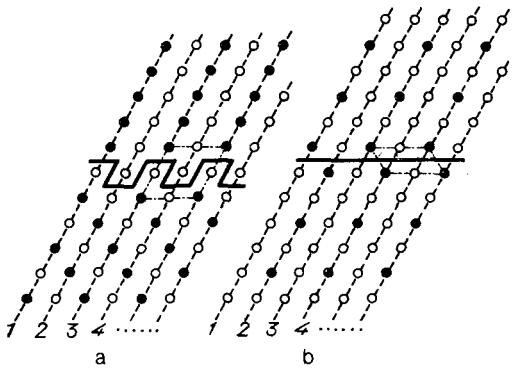


FIG. 12. Initial boundary configurations between two $2\times1$ (a) and two $2\times2$ (b) phases. The open circles and the black dots represent the $S=1$ and $S=-1$ spins, respectively; the continuous lines are domain walls the dashed lines are the columns labeled from 1 to $2N$; the chain line represents the unit cells in a local spin structure of the adjacent $2\times2$ (a) and $2\times1$ (b) phases.

we can expect a domain wall (representing the initial boundary configuration in the $2\times1$ phase) to have in a field $h_c = 2(1+\alpha)$ a local structure with zero energy of the $2\times2$ phase. Figure 12a shows such an initial configuration which is zigzag-shaped; it is described by $\{m_k, n_k\} = \{0,0,0,0,...\}$, where $m_k$ and $n_k$ are integers related to ther columns $2k-1$ and $2k$, respectively (the values of $k$ are 1, 2, 3, ..., $N$). The new boundary configurations can be obtained by shifting the boundary line in the columns $2k-1$ and $2k$ upward or downward by rotating a certain number of spins $m_k$ and $n_k$. Each such configuration is described by a set of integers $\{m_k, n_k\}$ with the sign governed by the shift of the boundary line relative to the initial line (where the minus sign corresponds to the downward shift). The boundary conditions are assumed to be periodic: $m_{N+k} = m_k$ and $n_{N+k} = n_k$. The energy of the initial configuration is

$$E_0 = -2(2J_1+2J_2+H)N \tag{4.1}$$

(the condition $E_0 = 0$ describes the expression for the critical field at zero temperatures). The energy of an arbitrary configuration with the set $\{m_k, n_k\}$, relative to $E_0$, is given by

$$\Delta E = -J_1 \sum_{k=1}^{N} [e^A(m_k, n_k) + e^B(n_k, m_{k+1})], \tag{4.2}$$

where

$$e^A(m, n) = 2(|n-m-1|-1) + 2\alpha(|n-m|-1) + h(n-m),$$

$$e^B(n, m) = 2(|m-n+1|-1) + 2\alpha(|m-n+2|-1) - h(m-n)$$

$$(h = H/J_1). \tag{4.3}$$

We shall now introduce the transfer matrix $T_{mm'}$ with the elements

$$T_{mm'} = \sum_{n=-\infty}^{\infty} \exp[J_1(e^A(m, n) + e^B(n, m'))\, T^{-1}]. \tag{4.4}$$

Using the properties of the translation symmetry of the transfer matrix $T_{mm'} = T_{m+1,m'+1}$, we can readily calculate its maximum eigenvalue $\lambda_{\max} = \Sigma_{m=-\infty}^{\infty} T_{m_0}$ and the free energy of interphase configurations $\mathcal{F} = E_0 - TN \ln \lambda_{\max}$. Assuming that $\mathcal{F} = 0$, we obtain the following equation for the phase transition line[103]:

$$(a_+ + b_-)(a_- + b_+) = 1, \tag{4.5}$$

where

$$a_\pm = \frac{\exp(-2\alpha/t)}{1-\exp[-(2+2\alpha\pm h)/t]},$$

$$b_\pm = \frac{\exp[-(2\pm h)/t]}{1-\exp[-(2+2\alpha\pm h)/t]}, \qquad t = \frac{T}{|J_1|}.$$

The line representing the boundary of the $2\times1$ phase is calculated from Eq. (4.5) for $\alpha = 0.5$ and 1, and is represented by curve 1 in Figs. 13a and 13b.

At finite temperatures we can readily find also the line of the transitions between the $2\times2$ and $1\times1$ phases. In the phase diagram of the ground states these phases are adjacent

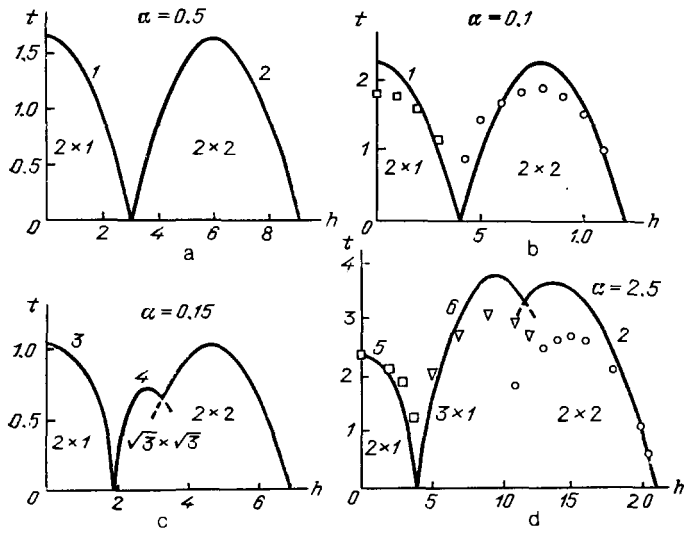


FIG. 13. Phase diagrams for different values of $\alpha$. Curves 1–6 represent transition lines between ordered states in the paramagnetic phase.[103] The results of numerical calculations carried out by the Monte Carlo method are shown for the values $\alpha = 1$ and 2.5 (b, d).[105]

on the high-field side. On the other hand, on the side of the low fields $h$ the $2\times2$ phase adjoins the $3\times1$, $2\times1$, and $\sqrt{3}\times\sqrt{3}$ phases (Fig. 9). However, at lower critical fields the initial zero-energy boundary configurations exist only in the form of a local spin structure analogous to the $2\times1$ phase; Fig. 12b shows such an initial configuration characterized by $\{m_k,n_k\}=\{0,0,0,0,\ldots\}$, with the energy $E_0=(2J_1+2J_2+H)N$. In the case of an arbitrary configuration the relative energy $\Delta E$ given in Eq. (4.2) by the terms with $e^A$ and $e^B$ is now described as follows:

$$e^A(m,n)=2[|n-m+1|-4(n-m)]+2\alpha[|n-m|-4(n-m)]+h(n-m)],$$

$$e^B(n,m)=2(|m-n|-1)+2\alpha(|m-n-1|-1)-h(m-n). \quad (4.6)$$

Since, as before, the transfer matrix with the terms given by Eq. (4.6) has translational symmetry, the free energy of a domain wall can be found analytically. Consequently, the equation for the transition lines can be represented in the form[103]

$$\left[a+b\exp\left(\frac{4}{t}\right)\right]\left[a+b\exp\left(\frac{4\alpha}{t}\right)\right]=\exp\left[\frac{2(1+\alpha)}{t}\right], \quad (4.7)$$

where

$$a=\frac{\exp[-(4+4\alpha-h)/2t]}{1-\exp[-(6+6\alpha-h)/t]}, \quad b=\frac{\exp(-h/2t)}{1-\exp[(2+2\alpha-h)/t]}.$$

The lines of the transitions of the $2\times2$ phase calculated from Eq. (4.7) for four different values of $\alpha$ are shown in Fig. 13 (curves labeled *2*).

In the phase diagrams of Figs. 13c and 13d we also find the phase transition lines (curves *3* and *5*) which correspond in the initial $2\times1$ phase to other types of boundary configurations, namely the configurations with the local spin structure $\sqrt{3}\times\sqrt{3}$ and with the $3\times1$ phases. Curves *4* and *6* in these figures are plotted for the case when initial $\sqrt{3}\times\sqrt{3}$ and $3\times1$ phases have boundary configurations with a local spin structure analogous to the $2\times1$ phase. Since for all these domain walls the elements of the transfer matrix have no translational symmetry, the *3*–*6* phase transition lines have to be found numerically. The maximum eigenvalue $\lambda_{\max}$ was calculated in Ref. 104 by the process of truncation of the $T_{mm'}$ matrix of infinite dimensions.

The results obtained by the interphase configuration method[102] reproduce correctly the phase transition lines *A*, *C*, *D*, and *E* for the ground state (Fig. 9) and there are no stable commensurate phases at any finite temperature on these lines. Initially, this is a consequence of the geometric nature of the local spin structure of a domain wall and is independent of the calculation details. On the other hand, since at $T=0$ there are no energy domain walls on the phase transition lines *B* and *F*, both phases are stable. Figures 13b and 13d show, for the sake of comparison, also the results of numerical calculations carried out by the Monte Carlo method.[105] It is clear from these figures that the phase diagrams found by the method of Ref. 102 are in good agreement with the Monte Carlo results. However, there are significant quantitative differences and this is clearly due to lack of allowance for the influence of the boundary configurations of finite size.

The phase diagram for the simpler case when $H>0$, $J_2>0$ ($\alpha<0$) can be found in Refs. 19 and 106–108. We shall conclude by noting the following: the problem of the possibility of existence of a partly disordered phase in two-dimensional systems is discussed in Ref. 109. In the mean field approximation such a partly disordered (PD) phase was predicted close to the critical fields $h_c=2(1+\alpha)$ between the $2\times1$ and $2\times2$ phases. However, it is well known that if fluctuations are large, the mean-field approximation can give even a qualitatively incorrect phase diagram, as in the case of two-dimensional systems with frustrated bonds.[107,110] Therefore, a better understanding and refinement of the phase diagram will require further investigations of this topic by more rigorous methods.

### 4.2. Phase transitions in Heisenberg antiferromagnets on a triangular lattice (anisotropic and limiting isotropic cases)

In the case of two-dimensional (2D) anisotropic Heisenberg ferromagnets described by the Hamiltonian

$$\mathcal{H}=-J_1\sum_{\mathbf{r}}(S_{\mathbf{r}}^xS_{\mathbf{r}+\mathbf{a}}^x+S_{\mathbf{r}}^yS_{\mathbf{r}+\mathbf{a}}^y)-J_1'\sum_{\mathbf{r}}S_{\mathbf{r}}^zS_{\mathbf{r}-\mathbf{a}}^z, \quad (4.8)$$

the coupling between the $xy$ spin components ($J_1\neq0$) stimulates ordering of the sublattices and induces (in contrast to the above case of pure Ising triangular systems with an antiferromagnetic interaction only between the nearest spins) a phase transition at $T\neq0$. Moreover, if in $J_1'=AJ_1$ the coefficient $A$ is greater than unity, there may be two consecutive phase transitions one of which is associated with the ordering of the $S^z$ spin component and the other with the ordering of $S^x$ and $S^y$.

In the case of an Ising-like Heisenberg antiferromagnet ($A>1$) the ground state represents three noncollinear (canted) magnetic sublattices lying in the same plane and this plane is oriented in an external field $\mathbf{H}=(0,0,H)$ in such a way that it includes the $z$ axis (vertical position). Such a system exhibits continuous degeneracy in respect of rotation of the plane by an angle $\varphi$ about the $z$ axis. In the plane itself the state with the minimum energy is described in the classical case of three sublattices by equations of the type[44]

$$\cos\theta_1(\sin\theta_2+\sin\theta_3)=A\sin\theta_1(\cos\theta_2+\cos\theta_3)-\frac{1}{3}h\sin\theta_1, \quad (4.9)$$

where $\theta_i$ are the sublattice angles in the range $[0,2\pi]$; $h=H/|J_1|$. The other two equations are obtained from the above by cyclic permutation of the indices.

We shall first consider the case when $H=0$. Then, out of three equations of the (4.9) type, only two are independent so that orientation of one of the sublattices $\theta_1$ is arbitrary. For each value of $\theta_1$ the other two sublattices become aligned in a nontrivial manner: the angles between the different sublattices have different values which vary with $\theta_1$. This situation resembles degeneracy of the ground state of a dipole system on a square lattice where again orientation of one of the four magnetic sublattices is arbitrary and the other three become aligned in a certain manner.[121] By way of ex-

TABLE I. Chiral symmetry and local order parameter of triangular antiferromagnets with different spins.

| Spin | Chirality | Local order parameter |
|---|---|---|
| Ising–Heisenberg[44] | $S_1$ | $S_1 \times S_1$ |
| Heisenberg[22] | $S_2$ | $P_3 = S_3/Z_2$ |
| $XY$ (Refs. 38–42) | $Z_2$ | $Z_2 \times S_1$ |

ample of stable states we can give the following solutions of equations of the (4.9) type: 1) $(\theta_1,\theta_2,\theta_3) = (0,\theta,\pi+\theta)$, where $\cos\theta = A/(1+A)$; 2) $(\theta_1,\theta_2,\theta_3) = (\pi/2,\theta,3\pi-\theta)$, where $\sin\theta = -1/(1+A)$. In both cases the ground-state energy is $E_0 = -(1+A+A^2)/(1+A)$. An examination of these two degenerate solutions shows that in the first case the angles between the sublattices are $\theta$, $\pi$, and $\pi-\theta$, whereas in the second case these angles are $\pi/2-\theta$, $\pi-\theta$, $\pi/2+2\theta$, i.e., they are indeed generally different and vary in an inequivalent manner. The system has a total angular momentum **M**, the orientation of which in the vertical plane is arbitrary and its modulus also decreases on reduction in $A$ and it vanishes for the isotropic case when $A = 1$ (this represents a structure with the 120° configuration of spins which remains unchanged also when $A < 1$). The states with noncollinear spins can be represented conveniently by what is known as the chiral vector[115]

$$\mathbf{k} = \frac{2}{3\sqrt{3}}([\mathbf{S}_1, \mathbf{S}_2] + [\mathbf{S}_2, \mathbf{S}_3] + [\mathbf{S}_3, \mathbf{S}_1]), \qquad (4.10)$$

where $\mathbf{S}_1$, $\mathbf{S}_2$, and $\mathbf{S}_3$ are unit vectors of the spins at the vertices of elementary triangles (the vertices 1, 2, and 3 are labeled clockwise; the modulus of the vector **k** vanishes when any two magnetic sublattices are parallel, but it is equal to unity for the 120° structure).

The ground state with two independent parameters $\varphi$ and $\theta_1$ is characterized by a degeneracy space $V = S_1 \times S_1$, which is not affected even in the harmonic approximation.[44] On the other hand, a continuous degeneracy in respect of the angle $\theta_1$ cannot be realized at $T \neq 0$ because of the different $(Z_6 \times S_1)$ symmetry of the Hamiltonian of Eq. (2.8).[2)]

Numerical calculations carried out for finite temperatures showed that the specific heat has anomalies at two points (for $A = 2$ these points are $T_1 = 0.9|J_1|$ and $T_2 = 0.3|J_1|$). Below the first transition point $T_1$ only $z$ components of the spin become ordered (this transition breaks the sixfold symmetry, so that the effective symmetry of the intermediate phase becomes $S_1$). In this state $(T_2 < T < T_1)$ the two sublattices of the spin structure become oriented opposite to the third, so that the net spin moment is zero. In the low-temperature phase $(T < T_2)$ the fluctuations of $\varphi$ are suppressed and correlations of the $xy$ components of the spin fall in accordance with a power law. The chiral vector **k** for this phase is finite. In fact, numerical experiments[44] have revealed a steep rise of **k** at the transition point $T = T_2$ [this is the $S \to R_1$ transition accompanied by the disappearance of free $Z$ vortices; $R_1$ is a straight line corresponding to a one-dimensional translation group $T(1)$]. The chiral symmetry and the local order parameter of triangular antiferromagnets with different spins are given in Table I.

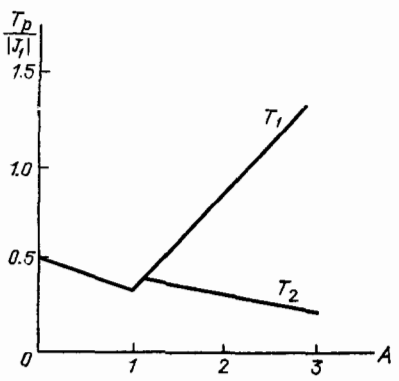


FIG. 14. Phase diagram of triangular 2D antiferromagnets with an anisotropic exchange interaction (based on Ref. 44); in the limit $A \to \infty$ the ratio is $T_1/A = 0$ (limiting case of an Ising system).

A reduction in $A$ reduces the temperature range of existence of the intermediate phase (Fig. 14) and it disappears for $A \lesssim 1$. In the isotropic limit when $A = 1$, the symmetry of the high-temperature phase changes from $Z_6 \times S_1$ to the projective space $P_3 = \mathrm{SO}(3)$, where SO(3) is the three-dimensional rotation group. Three-dimensional (3D) magnetic materials with the three-dimensional order parameter $V \sim \mathrm{SO}(3)$ are well known and these are primarily $UO_2$ and $YMnO_3$, and the superfluid phase (A) of $^3$He. In the case of two-dimensional frustrated systems considered here the only continuous transition is of the Berezinskiĭ–Kosterlitz–Thouless type and it is due to dissociation $(0 \to 1+1)$ of $Z_2$ vortex pairs. It is interesting to note that out of two types of vortices (Figs. 15a and 15b) the main contribution to thermodynamics is made by those $Z_2$ structures which are formed by rotation of the chiral vector around the core of a vortex (Fig. 15b), because they are the ones that have the lowest energy.[116] Two such $Z_2$ vortices, separated by a distance less than the spin correlation length, are characterized by opposite directions of rotation of the chiral vector in order to reduce the energy. They are thus very similar to a vortex–antivortex pair with opposite "charges" resembling $Z$ vortices in $XY$ ferromagnets.[3)] Table II gives, for the sake of comparison, data on topologically stable defects which appear in various spin systems with a 2D triangular lattice.

In contrast to the $S_1 \to R_1$ transition considered earlier, when the spin correlations obey a power law exactly as in the case of the ferromagnetic $XY$ model,[26–28] a topological $P_3 \to S_3$ transition in an isotropic antiferromagnet occurs between two phases each of which is characterized by an exponential falling off of the spin correlations. This can be understood, for example, **k** from the point of view of chiral symmetry. Below the critical temperature the continuous degree of freedom of the chiral vector **k** is conserved and its degeneracy space $S_2$ is identical with the space of the order

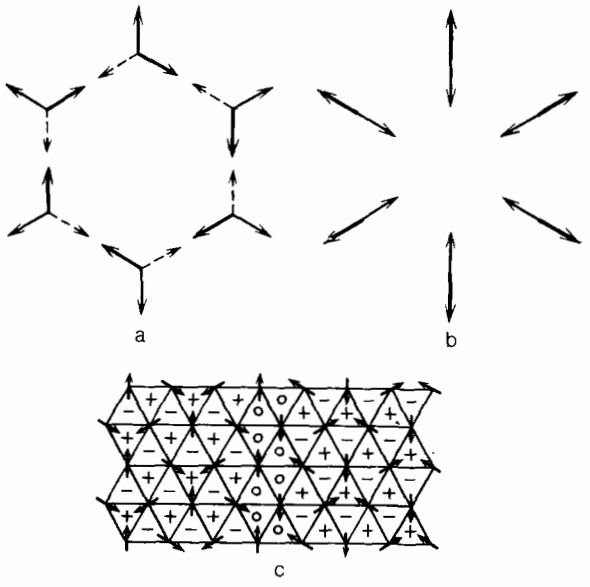


FIG. 15. a), b) $Z_2$ structures with a vortex number 1 in 2D Heisenberg triangular antiferromagnets; *a* represents a perpendicular orientation of the chiral vector relative to the plane of the figure, whereas *b* corresponds to the case when the chiral vector is in the plane of the figure (and one of the magnetic sublattices is perpendicular to the plane). c) Two ground states separated by a domain wall in a 2D $XY$ triangular antiferromagnet; the plus and minus signs correspond to the values $k = 1$ and $k = -1$; $k = 0$ along the wall.

parameter of a Heisenberg ferromagnet. In the case of such a ferromagnet the spin correlations again fall off exponentially at any finite temperature,[114] but the Berezinskiĭ–Kosterlitz–Thouless phase transition does not occur because topological excitations known as instantons (Table II) have only a finite energy independent of the size of the system.

Kawamura and Miyashita demonstrated[22] that the order parameter of such a system can be introduced via a vortex function defined on a closed contour.[22] In a high-temperature phase a vortex function falls off rapidly in accordance with the area law, whereas in a low-temperature phase it falls more slowly in accordance with the perimeter law. This phase transition criterion resembles the criterion used in the problem of quark confinement in the lattice gauge theory.[29,30]

Consecutive phase transitions have been observed experimentally in a precision study of the quasi-two-dimensional Heisenberg antiferromagnet $VCl_2$ (Ref. 123). In view of a weak Ising anisotropy this material exhibits consecutive phase transitions at $T_1 = 35.88$ K and $T_2 = 35.80$ K. In the 2D Heisenberg range, just above $T_1$, the line profile of the susceptibility $\chi(\mathbf{q})$ is close to the Ornstein–Zernike function, which confirms the presence of magnetic point defects in the system. On the other hand, a different quasi-two-dimensional Heisenberg ferromagnet in the form of $VBr_2$ exhibits just one transition. As in the case of numerical calculations relating to the isotropic case characterized by $A = 1$, the temperature dependence of the homogeneous susceptibility near the critical point is then almost flat and isotropic.[31,34]

It should be pointed out here that the compounds $VBr_2$ and $VCl_2$ are characterized by a weak interplanar interaction and this results in a crossover from the 2D to the 3D behavior with temperature. Thermal, magnetic, and neutron diffraction studies of these compounds carried out in the narrow 3D temperature range show that their critical behavior differs considerably from that usual in the case of unfrustrated systems with the $Z_2$, $S_1$, or $S_2$ symmetry: the specific heat of $VBr_2$ is characterized by a strong divergence[122] ($\alpha = 0.59$) and the values of $\beta = 0.20$, $\gamma = 1.05$, and $\nu = 0.62$ for $VCl_2$ (Ref. 123) are close to the critical exponents of the SO(3) universal class calculated recently in Ref. 35 (Table III). It would therefore be interesting to investigate the critical behavior (in the case of continuous transitions) for other magnetic materials characterized by the three-dimensional order parameter $V \sim SO(3)$, such as $YMnO_3$ or the A superfluid phase of $^3He$. The main problem in detection of new critical behavior of these materials is the small width of the critical region. This is particularly true of the $^3He$-A phase with an extremely narrow critical region[124] of width of the order of $t \sim 10^{-5}$; only a finite jump of the specific heat has been observed experimentally[23] (which represents meanfield behavior outside the interval $t$), whereas observation of the expected diverging specific heat $C$ would require measurements of very high precision.

The nontrivial degeneracy of the ground state with respect to $\theta_1$ (when $A > 1$) disppears in an external field $H \neq 0$. Depending on the value of $H$, four stable planar configurations can be expected (Figs. 16a–16d). These configurations satisfy the following solutions of the system of equations (4.9):

$$\begin{aligned}
&\text{a)}\ \theta_1 = \pi,\ \theta_2 = -\theta_3 = \theta, \quad \cos\theta = \left(A + \frac{h}{3}\right)(1+A)^{-1}, \quad 0 \leqslant h \leqslant h_{c_1},\\
&\text{b)}\ \theta_1 = \pi,\ \theta_2 = \theta_3 = 0, \quad h_{c_1} \leqslant h \leqslant h_{c_2},\\
&\text{c)}\ \theta_1 \neq \theta_2 = \theta_3, \quad h_{c_2} \leqslant h \leqslant h_{c_3},\\
&\text{d)}\ \theta_1 = \theta_2 = \theta_3, \quad h \geqslant h_{c_3},
\end{aligned} \tag{4.11}$$

TABLE II. Space of the order parameter $V$ and associated homotopic group $\pi_r(V)$ for different spin systems with triangular lattices.

| System | $V$ | $\pi_0(V)$ | $\pi_1(V)$ | $\pi_2(V)$ |
|---|---|---|---|---|
| | Order parameter space | Line | Point | Instanton |
| Ferromagnetic $XY$ | $S_1 = SO(2)$ | 0 | $Z$ | 0 |
| Ferromagnetic Heisenberg | $S_2$ | 0 | 0 | $Z$ |
| Antiferromagnetic Heisenberg | $P_3 = SO(3)$ | 0 | $Z_2$ | 0 |
| Antiferromagnetic $XY$ | $Z_2 \times S_1$ | $Z_2$ | $Z$ | 0 |

TABLE III. Values of critical exponents for different three-dimensional systems (values for systems $Z_2$, $S_1$, and $S_2$ taken from Ref. 125).

| System | $\alpha$ | $\beta$ | $\gamma$ | $\nu$ |
|---|---|---|---|---|
| Ising ($Z_2$) | 0.110 | 0.325 | 1.240 | 0.630 |
| $XY$ ($S_1$) | −0.008 | 0.346 | 1.316 | 0.669 |
| Heisenberg ($S_2$) | −0.116 | 0.365 | 1.387 | 0.705 |
| Antiferromagnetic Heisenberg [SO(3)](Ref.35) | 0.4 | 0.25 | 1.1 | 0.53 |
| Antiferromagnetic $XY$ ($Z_2 \times S_1$) (Ref. 42) | 0.44 | 0.22 | 1.1 | 0.52 |

where $h_{c_1} = 3$, $h_{c_2} = 1.5[2A - 1 + [4A^2 + 4A - 7)^{1/2}]$, $h_{c_3} = 3(1 + 2A)$. The temperature dependences of the magnetization curves $M_z(H_z)$ and $M_x(H_z)$ are shown in Fig. 16(e) (on the assumption that the plane of the spin configurations coincides with the $z$, $x$ plane). The $M_z(H_z)$ curve exhibits "metamagnetic" behavior, in contrast to a planar triangular antiferromagnet[39] in which case it should be a straight line until $M_z$ reaches its saturation value. By analogy with the Ising case,[106,126] the $M_z(H_z)$ curve has a plateau at a height of 1/3 of $M$. This plateau corresponds to the structure shown in Fig. 16b within the range of fields $h_{c_1} \leqslant h \leqslant h_{c_2}$; in the isotropic limit characterized by $A = 1$ the range $h$ contracts to a point. The other curve $M_x(H_z)$ is due to the existence of a nontrivial degree of freedom in the direction of $x$ exhibited by one of the states (Fig. 16c).

The T–H phase diagram of anisotropic Heisenberg antiferromagnets has been investigated before.[127,128] This diagram consists of three ordered phases $a$, $b$, and $c$ (Figs. 17a and 17b) and the high-temperature phase ($c$) has the $Z_3 \times S_1$ symmetry. In the intermediate fields, even when $A = 1$ (Fig. 17a), there may be two consecutive phase transitions, one of which is associated with the ordering of the longitudinal components of the spin and the other with the ordering of the transverse components. The phases $a$ and $c$ have the same $R_1$ symmetry, but in contrast to the phase $a$ the chiral vector of the phase $c$ vanishes because the two sublattices are parallel. An increase in $A$ reduces the range of existence of the phases $a$ and $c$ (Fig. 17b) and this range disappears in the limiting case of a pure Ising system (Fig. 17c).

In the case of frustrated systems the quantum effects may alter the ground state decisively and this is essentially due to the feasibility of complete disappearance of the effective spin length. This circumstance is particularly important in the case of Heisenberg antiferromagnets with spin 1/2, when the ground state can be described (as suggested by Anderson) by a model of a magnetic quantum liquid representing an ensemble of randomly distributed mobile singlet pairs on a two-dimensional triangular lattice.[45] Such a ground state is characterized by resonating valence bonds[45] and it has been confirmed (at least partly) by numerical calculations for finite systems.[129,130] Moreover, Fazekas and Anderson[131] demonstrated that the resonating valence bond state may be invoked conveniently even in describing the ground state of systems with an Ising-like exchange anisotropy. Thermodynamic properties of such systems are considered in Ref. 132 for the case when $H = 0$: in contrast to classical systems, they do not exhibit ordered sublattices or phase transitions. Real experiments on two-dimensional Heisenberg $NaTiO_2$ and Ising-like $LiNiO_2$ antiferromagnets have also failed to reveal any long-range order[46,87] (it was found that Bragg scattering does not occur even at very low temperatures).

The problem of the ground state of anisotropic Heisenberg antiferromagnets with $S = 1/2$ subjected to an external

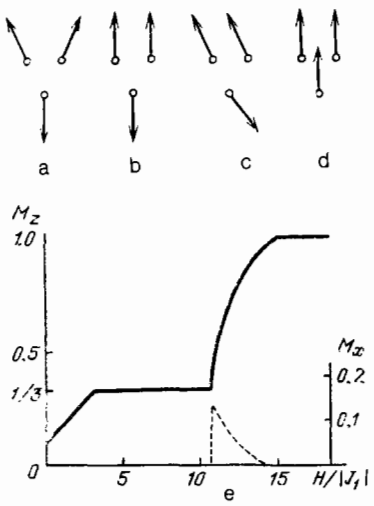


FIG. 16. a)–d) Ground state of an Ising-like Heisenberg antiferromagnet in different fields: a) $0 \leqslant h \leqslant h_{c_1}$; b) $h_{c_1} < h < h_{c_2}$; c) $h_{c_2} < h < h_{c_3}$; d) $h > h_{c_3}$. e) Magnetization curves in units of $M$ plotted for the case when $A = 2$; the continuous curve represents $M_z(H_z)$ and the dashed curve gives $M_x(H_z)$ (Ref. 128).

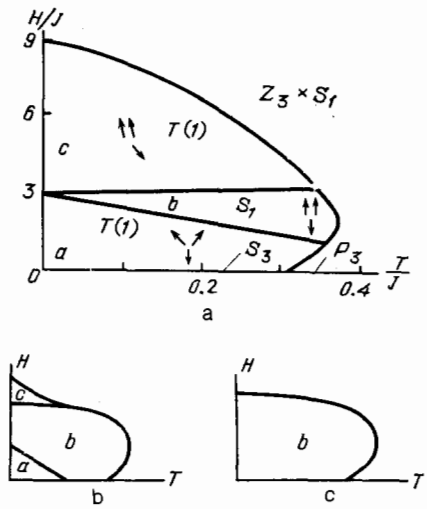


FIG. 17. Phase diagrams (b and c are schematic) of two-dimensional triangular antiferromagnets: a) isotropic case case[127], b) anisotropic case[128]; c) limiting case of an Ising system.

field was investigated by Nishimori and Miyashita.[47] They determined the dependence of $M_z$ on $H_z$ by numerical diagonalization of the spin Hamiltonian of Eq. (4.8). The results of the calculations showed that in fields $H \to 0$ the magnetization $M_z$ is unlikely to remain finite, which is in contrast to the classical case. Moreover, in the range of fields $h_{c_1} \leqslant h \leqslant h_{c_2}$ there is a plateau (at the same height of 1/3 of $M$) also in the case of a quantum system. so that in this range of $h$ the classical state with collinear spins (Fig. 16b) predominates. Outside the plateau the system is effectively in a quantum state. In particular, the classical description ceases to be valid in the range $h > h_{c_2}$, where the transverse magnetization shows no long-range order—the state with the skew sublattices (Fig. 16c) is suppressed—and we have everywhere $M_x(H_z) = 0$.

### 4.3. Phases in a triangular planar antiferromagnetic

In the case of frustrated antiferromagnets with the $XY$ spins on a triangular lattice we can expect not only a continuous degeneracy of the ground state, but also a double discrete degeneracy: the two ground states with mutually opposite orientations of the wave vector $\mathbf{Q}_k$ of a 120° structure cannot be converted into one another by rotation of spins in a plane (Fig. 15c). Since the space $V$ of such systems is characterized by the $O(2) = Z_2 \times S_1$ symmetry, we can expect—by analogy with the results in the previous section—two phase transitions with consecutive disturbance of the discrete and continuous components of the order parameter.

A phase transition in zero magnetic field has been investigated on many occasions for systems of this kind.[38-41] The first numerical calculations reported in Ref. 38 demonstrated that the critical temperatures due to the presence of linear and point defect systems are very similar. Moreover, further numerical calculations[39] show that, within the limits of statistical error, these critical temperatures are identical because of the mechanism of vortex distribution by domain walls. A similar result predicting a single transition was obtained also by other methods.[40,41]

An external field applied in the plane of a triangular lattice induces a continuous degeneracy of the ground state in the range $H < 9|J_1|$ (because the opposite inequality $H \geqslant 9|J_1|$ corresponds to the parallel orientation of the spins representing collapsed sublattices). Moreover, if $H < 3|J_1|$ the discrete symmetry is also retained, i.e., in other words, there are two uncoupled sets of states. However, the continuous degree of freedom is not due to the symmetry of the Hamiltonian of the system ($H \neq 0$):

$$\mathcal{H} = -J_1 \sum_{\mathbf{r}} \mathbf{S}_{\mathbf{r}} \mathbf{S}_{\mathbf{r}+\mathbf{a}} - \sum_{\mathbf{r}} \mathbf{H}\mathbf{S}_{\mathbf{r}}, \tag{4.12}$$

because at finite temperatures it should not be allowed.

In the presence of a magnetic field, the symmetry group of $\mathcal{H}$ in Eq. (4.12) is

$$G = \mathbf{T} \cdot C_{6v} \cdot C_s^{(\mathrm{spin})}, \tag{4.13}$$

where $\mathbf{T} = m\mathbf{a}_1 + n\mathbf{a}_2$ and $C_6v$ are, respectively, the translation group and the point group on a triangular lattice; $C_s^{(\mathrm{spin})}$ is a group related to the reflection of spin relative to the direction of the magnetic field. The Fourier component of the spin

$$\psi_{\mathbf{Q}_k} = N^{-1} \sum_{\mathbf{R}} \mathbf{S}_{\mathbf{R}} \exp(-i\mathbf{Q}_k\mathbf{R}) \equiv (\sigma_\parallel + i\tau_\parallel, \sigma_\perp + i\tau_\perp) \tag{4.14}$$

($\sigma_\parallel$, $\tau_\parallel$ and $\sigma_\perp$, $\tau_\perp$ are, respectively, the longitudinal and transverse components relative to the orientation of $\mathbf{H}$), corresponding to the order parameter, forms a four-dimensional basis ($\sigma_\parallel, \tau_\parallel, \sigma_\perp, \tau_\perp$) in which the irreducible representation of the group $G$ consists of twelve elements. However, since matrices of such a representation have the block diagonal form, they can be reduced to matrices of two irreducible representations with the bases ($\sigma_\parallel, \tau_\parallel$) and ($\sigma_\perp, \tau_\perp$); in this case the first basis admits only six different matrices, whereas the second basis admits twice the number of matrices because of spin reflections relative to the field. An analysis of the transformations made using the group $G$ elements shows that the matrices of the representations with the ($\sigma_\parallel, \tau_\parallel$) basis are isomorphous with the point group $C_{3v}$, whereas in the ($\sigma_\perp, \tau_\perp$) case they are isomorphous with $C_{6v}$ [($C_{3v}, C_{6v}$) is the representation of the initial phase].

Table IV lists all six subgroups of the group $G$ (it is assumed that the largest translation period is exhibited by the $\sqrt{3} \times \sqrt{3}$ structure); this table includes also nonzero components of the order parameter for the various subgroups obtained by a group-theoretic analysis. In general, when the spin ($S$), $1 \times 1$ translation ($T$), and point ($P$) symmetries break down, we can use eleven continuous transitions between the various subgroups for which the representations are given in Table IV; the list of these subgroups is as follows:

TABLE IV. Subgroups of the space group $G$ and corresponding order parameter components of planar antiferromagnetic systems with triangular lattices.[39]

| Spin group | Translation group | Point group | Representation | Order parameter | | | |
|---|---|---|---|---|---|---|---|
| | | | | $\lvert\langle\sigma_\parallel\rangle\rvert$ | $\lvert\langle\tau_\parallel\rangle\rvert$ | $\lvert\langle\sigma_\perp\rangle\rvert$ | $\lvert\langle\tau_\perp\rangle\rvert$ |
| $C_s$ | $m\mathbf{a}_1 + n\mathbf{a}_2$ | $C_{6v}$ | ($C_{3v}$, $C_{6v}$) | 0 | 0 | 0 | 0 |
| $I$ | $m\mathbf{a}_1 + n\mathbf{a}_2$ | $C_{6v}$ | ($C_{3v}$, $C_{3v}$) | 0 | 0 | 0 | 0 |
| $C_s$ | $(m+2n)\mathbf{a}_1 + (m-n)\mathbf{a}_2$ | $C_{6v}$ | ($C_s$, $C_{2v}$) | $>0$ | 0 | 0 | 0 |
| $I$ | $(m+2n)\mathbf{a}_1 + (m-n)\mathbf{a}_2$ | $C_{6v}$ | ($C_s$, $C_s$) | $\geqslant 0$ | 0 | $>0$ | 0 |
| $C_s$ | $(m+2n)\mathbf{a}_1 + (m-n)\mathbf{a}_2$ | $C_{3v}$ | ($C_1$, $C_i$) | $\geqslant 0$ | $>0$ | 0 | 0 |
| $I$ | $(m+2n)\mathbf{a}_1 + (m-n)\mathbf{a}_2$ | $C_{3v}$ | ($C_1$, $C_1$) | $\begin{cases} \geqslant 0 \\ >0 \end{cases}$ | $\begin{cases} \geqslant 0 \\ >0 \end{cases}$ | $\begin{cases} \geqslant 0 \\ >0 \end{cases}$ | $\begin{cases} >0 \\ 0 \end{cases}$ |

1) $(C_{3v}, C_{6v}) \to (C_{3v}, C_{3v})$, 2) $(C_{3v}, C_{6v}) \to (C_s, C_{2v})$,
3) $(C_{3v}, C_{3v}) \to (C_s, C_s)$,
4) $(C_s, C_{2v}) \to (C_s, C_s)$, 5) $(C_s, C_{2v}) \to (C_1, C_1)$,
6) $(C_s, C_s) \to (C_1, C_1)$,
7) $(C_1, C_1) \to (C_1, C_1)$,
8) $(C_{3v}, C_{6v}) \to (C_s, C_s)$, 9) $(C_{3v}, C_{6v}) \to (C_1, C_1)$,
10) $(C_s, C_{2v}) \to (C_1, C_1)$, 11) $(C_{3v}, C_{6v}) \to (C_1, C_1)$.

(4.15)

Of all the cases listed above transition 1, characterized by symmetry breaking relative to spin reflections, is unique and in this case the order parameter of Eq. (4.14) is unimportant. Obviously, this is related physically to conservation of the $1 \times 1$ translation symmetry. On the other hand, transitions 8 and 9 involve simultaneous breaking of two symmetries: either the $S$ and $T$ symmetries in the case of transition 8 or the $T$ and $P$ symmetries in the case of transition 9; transition 11 is accompanied by breaking of all three symmetries $S$, $T$, and $P$.

A numerical investigation of the field dependence of the components of the order parameter at various temperatures shows that there are four second-order transition lines: two are of the order–disorder type and the other two are of the order–order type.[39] Figure 18 shows the ranges of existence of the various phases with nonzero components $\langle\sigma\rangle$ and $\langle\tau\rangle$. As in the case of anisotropic Heisenberg ferromagnets (Sec. 4.2), there are three ordered phases. The symmetries of these phases are found from Table IV. In the range $H \leqslant 4|J_1|$ an ordered state is characterized by $\langle\sigma_\parallel\rangle \neq 0$ (with the chiral parameter $k = 0$) and has the $(C_s, C_{2v})$ symmetry; cooling causes additional condensation to either the transverse component $\langle\tau_\perp\rangle$ [when $k \neq 0$, representing the $(C_1, C_1)$ phase] or $\langle\sigma_\perp\rangle$ [$k = 0$, $(C_s, C_s)$ phase]. Consequently, if $H < 3|J_1|$, we can expect consecutive phase transitions $(C_{3v}, C_{6v}) \to (C_s, C_{2v}) \to (C_1, C_1)$, whereas in the case when $3|J_1| < H \lesssim 4|J_1|$, we can expect transitions $(C_{3v}, C_{6v}) \to (C_s, C_{2v}) \to (C_s, C_s)$. These and other transitions are in agreement with those deduced from the symmetry analysis represented by Eq. (4.15).

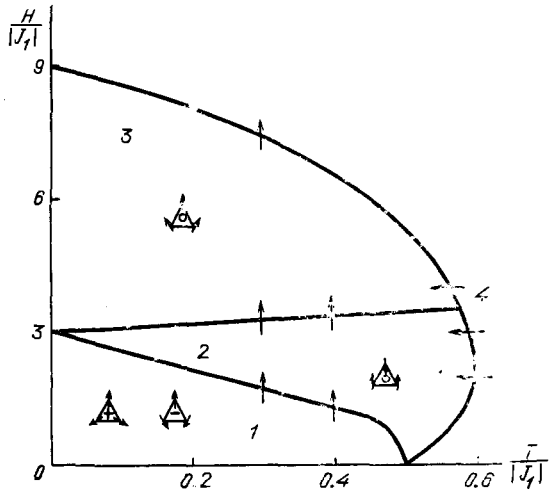


FIG. 18. Phase diagram of planar antiferromagnetic systems with triangular lattices[39]: 1) $(C_1, C_1)$ phase with the order parameter components $\langle\sigma_\parallel\rangle \neq 0$, characterized by $\langle\tau_1\rangle \neq 0$ and by the chiral vector $k \neq 0$; 2) $(C_s, C_{2v})$ phase with $\langle\sigma_\parallel\rangle \neq 0$, $k = 0$; 3) $(C_s, C_s)$ phase with $\langle\sigma_\parallel\rangle \neq 0$, $\sigma_\perp \neq 0$, $k = 0$; 4) $(C_{3v}, C_{6v})$ phase with $\langle\sigma_{\parallel,\perp}\rangle = 0$ and $\langle\tau_{\parallel,\perp}\rangle = 0$. The arrows in the phase diagrams indicate the directions of the transitions, the critical behavior of which was investigated at fixed values of $H$ or $T$.

The phase boundaries have been investigated in an external field on the basis of the symmetry and scaling calculations made by the Monte Carlo method in the case of finite systems.[118–120] The scaling curves of the $(C_{3v}, C_{6v}) \to (C_s, C_{2v})$ transition when $H = 2|J_1|$ and $H = 3|J_1|$ (Fig. 18) are described well by the critical exponents $\alpha = 1/3, \beta = 1/9, \gamma = 13/9, \nu = 5/6$ (Ref. 39), which have the same values as for a transition belonging to a universal class of a three-level Potts model.[133] On the other hand, the nature of the transition at the other boundaries is quite different. For example, similar calculations of the critical exponents along the boundary representing the $(C_{3v}, C_{6v}) \to (C_s, C_s)$ phase transition exhibit nonuniversal behavior[39]: it is found that if $H = 4|J_1|$, then $\beta = 0.20$ and $\gamma = 1.55$, whereas for $T = -0.3|J_1|$, we have $\beta = 0.28$ and $\gamma = 1.45$ (in both cases we have $\nu = 1$; the specific heat shows no divergence: $\alpha < 0$). A nonuniversal behavior is exhibited also by two internal phase boundaries associated with the $(C_1, C_1) \to (C_s, C_{2v})$ and $(C_s, C_s)$ transitions when an increase in the temperature from $T = 0.3\,|J_1|$ to $T = 0.4\,|J_1|$ increases the value of $\beta$ from 0.14 to 0.21. In the case of the last transition it is interesting to note that the specific heat shows no anomalies on crossing the $(C_s, C_{2v}) \to (C_s, C_s)$ boundary, and the homogeneous magnetization shows no singularities, so that the phase transition can be detected only on the basis of the behavior of the order parameter.

An experimental investigation of a phase transition in an external field was reported in Ref. 111 for the planar quasi-two-dimensional triangular antiferromagnet $CsMnBr_3$. It was found there that the only phase transition split into two on application of a field $H \neq 0$. The critical behavior of $CsMnBr_3$ was also investigated recently in the 3D region of the temperature crossover ($H = 0$). The experimentally determined[112,113] critical exponents of this compound differ considerably from those of standard unfrustrated systems, but they are close to the corresponding exponents of the $Z_2 \times S_1$ universal class calculated theoretically in Refs. 42 and 134 (Table III).

In the case of two-dimensional quantum systems with spin $S = 1/2$ spin no phase transition has been found at $T \neq 0$ and this is true of both the $XY$ antiferromagnets and of the Heisenberg ferromagnets. However, numerical results obtained for the ground state[36] demonstrate a falling off of the correlation function in accordance with the power law with an exponent $\eta = 0.34$.

## 5. CONCLUSIONS

The reported experimental and theoretical investigations of antiferromagnets with a triangular lattice have revealed many interesting and very different phases and phase transitions. The properties of the phases and the behavior of ferromagnetic systems in the course of ordering are very different from conventional materials and the differences are essentially due to the fact that the systems are frustrated.

This accounts also for the high sensitivity of the order parameter to various perturbations. Further investigations would be desirable to find the role of other possible factors. One of them is the influence of impurities on thermodynamic properties of frustrated systems. Even a slight random distortion of a triangular lattice by impurities (and the associated change in the exchange interaction constants) can have significant effects. Another factor is the stability of a triangular lattice in the presence of regular deformations. Frustrations in two-dimensional antiferromagnets may be allowed because of distortions of an equilateral triangular lattice to an isosceles lattice, which corresponds to an antiparallel configuration of the spins along one of the directions. This instability is essentially of the spin-Peierls nature, which usually appears in quasi-one-dimensional antiferromagnetic systems. It would also be interesting to investigate how the properties of a quantum magnetic liquid change in the presence of three-dimensional effects due to the interplanar exchange interaction. It would also be very important to carry out a more extensive investigation of the dynamic properties of frustrated systems and particularly of two-dimensional Heisenberg antiferromagnets because their low-temperature phase exhibits a large (though finite) length of spin correlations. Undoubtedly, further active studies of antiferromagnets with triangular lattices will yield many other interesting results and this will help in a better understanding of this great variety of the properties of these systems.

The author is deeply grateful to Yu. A. Izyumov for discussing this review, to M. I. Kaganov, A. V. Chubukov, and E. V. Kuz'min for reading the manuscript and valuable comments. It is a pleasure to thank B. A. Ivanov for valuable advice included in this paper. Finally, I am indebted to V. A. Ignatchenko for encouraging the writing of this review and discussing the organization of the paper and its content.

[1)]The structure of such a surface is similar to the potential surface of doubly degenerate states in the Jahn–Teller effect.[54,55]

[2)]In principle, in some cases an increase in the symmetry at the critical points on the phase diagram is also possible and this is known as the asymptotic symmetry.[117]

[3)]If the distance between the $Z_2$ vortices is greater than the spin correlation length, this analogy of course does not apply because the spin waves destroy all the nontopological characteristics of the vortices.

[1]T. Haseda, N. Wada, M. Hata, and K. Amaya, Physica B + C (Utrecht) **108**, 841 (1981).
[2]N. Wada, K. Ubukoshi, and K. Hirakawa, J. Phys. Soc. Jpn. **51**, 2833 (1982).
[3]H. Shiba, Solid State Commun. **41**, 511 (1982).
[4]N. Suzuki, J. Phys. Soc. Jpn. **52**, 3199 (1983).
[5]W. Knop, M. Steiner, and P. Day, J. Magn. Magn. Mater. **31–34**, 1033 (1983).
[6]N. V. Fedoseeva, R. S. Gekht, T. A. Velikanova, and A. D. Balaev, Pis'ma Zh. Eksp. Teor. Fiz. **41**, 332 (1985) [JETP Lett. **41**, 406 (1985)].
[7]Yu. A. Izyumov, Usp. Fiz. Nauk **144**, 439 (1984) [Sov. Phys. Usp. **27**, 845 (1984)].
[8]Yu. A. Izyumov, *Neutron Diffraction by Long-Period Structures* [in Russian], Énergoatomizdat, M., 1987.
[9]A. Adam, D. Billerey, C. Terrier, R. Mainard *et al.*, Solid State Commun. **35**, 1 (1980).
[10]S. R. Kuindersma, J. P. Sanchez, and C. Haas, Physica B (Utrecht) **111**, 231 (1981).
[11]L. P. Regnault, J. Rossat-Mignod, A. Adam, D. Billerey, and C. Terrier, J. Phys. (Paris) **43**, 1283 (1982).
[12]A. Adam, D. Billerey, C. Terrier, H. Bartholin, L. P. Regnault, and J. Rossat-Mignod, Phys. Lett. A **84**, 24 (1981).
[13]M. W. Moore, P. Day, C. Wilkinson, and K. R. A. Ziebeck, Solid State Commun. **53**, 1009 (1985).
[14]J. Villain, Physica B (Utrecht) **86–88**, 631 (1977).
[15]R. S. Gekht, Zh. Eksp. Teor. Fiz. **93**, 255 (1987) [Sov. Phys. JETP **66**, 147 (1987)].
[16]H. Yoshizawa and K. Hirakawa, J. Phys. Soc. Jpn. **46**, 448 (1979).
[17]W. B. Yelon, D. E. Cox, and M. Eibschütz, Phys. Rev. B **12**, 5007 (1975).
[18]H. Shiba, Prog. Theor. Phys. **64**, 466 (1980).
[19]M. Kaburagi, T. Tonegawa, and J. Kanamori, J. Phys. Soc. Jpn. **51**, 3857 (1982).
[20]F. Matsubara and S. Ikeda, Phys. Rev. B **28**, 4064 (1983).
[21]F. Matsubara and S. Inawashiro, J. Phys. Soc. Jpn. **53**, 4373 (1984).
[22]H. Kawamura and S. Miyashita, J. Phys. Soc. Jpn. **53**, 9 (1984).
[23]D. Fruchart, E. F. Bertaut, R. Madar, G. Lorthioir, and R. Fruchart, Solid State Commun. **9**, 1793 (1971).
[24]A. F. Andreev and V. I. Marchenko, Usp. Fiz. Nauk **130**, 39 (1980) [Sov. Phys. Usp. **23**, 21 (1980)].
[25]J. C. Wheatley, Rev. Mod. Phys. **47**, 415 (1975).
[26]V. L. Berezinskiĭ, Zh. Eksp. Teor. Fiz. **59**, 907 (1970) [Sov. Phys. JETP **32**, 493 (1971)].
[27]J. M. Kosterlitz and D. J. Thouless, J. Phys. C **6**, 1181 (1973).
[28]J. M. Kosterlitz, J. Phys. C **7**, 1046 (1974).
[29]K. G. Wilson, Phys. Rev. D **10**, 2445 (1974).
[30]J. B. Kogut, Rev. Mod. Phys. **51**, 659 (1979).
[31]K. Hirakawa, H. Kadowaki, and K. Ubukoshi, J. Phys. Soc. Jpn. **52**, 1814 (1983).
[32]K. Hirakawa, H. Ikeds, H. Kadowaki, and K. Ubukoshi, J. Phys. Soc. Jpn. **52**, 2882 (1983).
[33]I. Yamada, K. Ubukoshi, and K. Hirakawa, J. Phys. Soc. Jpn. **53**, 381 (1984).
[34]K. Takeda, K. Ubukoshi, T. Haseda, and K. Hirakawa, J. Phys. Soc. Jpn. **53**, 1480 (1984).
[35]H. Kawamura, J. Phys. Soc. Jpn. **54**, 3220 (1985).
[36]H. Nishimori and H. Nakanishi, J. Phys. Soc. Jpn. **57**, 626 (1988).
[37]E. Rastelli and A. Tassi, J. Phys. C **21**, L35 (1988).
[38]S. Miyashita and H. Shiba, J. Phys. Soc. Jpn. **53**, 1145 (1984).
[39]D. H. Lee, J. D. Joannopoulos, J. W. Negele, and D. P. Landau, Phys. Rev. Lett. **52**, 433 (1984); Phys. Rev. B **33**, 450 (1986).
[40]M. Yosefin and E. Domany, Phys. Rev. B **32**, 1778 (1985).
[41]M. Y. Choi and D. Stroud, Phys. Rev. B **32**, 5773 (1985).
[42]H. Kawamura, J. Phys. Soc. Jpn. **55**, 2095 (1986).
[43]R. S. Gekht, Zh. Eksp. Teor. Fiz. **87**, 2095 (1984); [Sov. Phys. JETP **60**, 1210 (1984)].
[44]S. Miyashita and H. Kawamura, J. Phys. Soc. Jpn. **54**, 3385 (1985).
[45]P. W. Anderson, Mater. Res. Bull. **8**, 153 (1973).
[46]K. Hirakawa, H. Kadowaki, and K. Ubukoshi, J. Phys. Soc. Jpn. **54**, 3526 (1985).
[47]H. Nishimori and S. Miyashita, J. Phys. Soc. Jpn. **55**, 4448 (1986).
[48]E. Rastelli and A. Tassi, J. Phys. C **19**, L423 (1986); E. Rastelli, L. Reatto, and A. Tassi, J. Phys. C **19**, L589 (1986).
[49]E. Rastelli and A. Tassi, J. Phys. C **20**, L303 (1987).
[50]G. C. De Fotis, Phys. Rev. B **23**, 4714 (1981).
[51]K. Nakanishi and H. Shiba, J. Phys. Soc. Jpn. **51**, 2089 (1982).
[52]Y. Ishibashi and V. Dvorak, J. Phys. Soc. Jpn. **45**, 1119 (1978).
[53]A. Aharony and M. E. Fisher, Phys. Rev. B **8**, 3323 (1973).
[54]H. A. Jahn and E. Teller, Proc. R. Soc. London Ser. A **161**, 220 (1937).
[55]S. Krupička, *Physik der Ferrite und der verwandten Magnetischen Oxide*, Vieweg, Brunswick, West Germany (1973). [Russ. transl., Mir, M., 1976]
[56]H. Shiba and N. Suzuki, J. Phys. Soc. Jpn. **51**, 3488 (1982).
[57]T. K. Soboleva, E. P. Stefanovskiĭ, and V. V. Tarasenko, Fiz. Tverd. Tela (Leningrad) **22**, 2353 (1980) [Sov. Phys. Solid State **22**, 1370 (1980)].
[58]C. S. O. Yokoi, M. D. Coutinho-Filho, and S. R. Salinas, Phys. Rev. B **24**, 4047 (1981).
[59]Yu. A. Izyumov, V. M. Laptev, and S. B. Petrov, Fiz. Tverd. Tela (Leningrad) **26**, 734 (1984) [Sov. Phys. Solid State **26**, 443 (1984)].
[60]I. E. Dzyaloshinskiĭ, Zh. Eksp. Teor. Fiz. **47**, 992 (1964) [Sov. Phys. JETP **20**, 665 (1965)].
[61]W. L. McMillan, Phys. Rev. B **14**, 1496 (1976).
[62]P. G. de Gennes, *The Physics of Liquid Crystals*, Clarendon Press, Oxford (1974). [Russ. transl., Mir, M., 1977]
[63]T. A. Kontorova and Ya. I. Frenkel', Zh. Eksp. Teor. Fiz. **8**, 1340 (1938).
[64]L. N. Bulaevskiĭ and D. I. Khomskiĭ, Zh. Eksp. Teor. Fiz. **74**, 1863 (1978) [Sov. Phys. JETP **47**, 971 (1978)].
[65]V. L. Pokrovskiĭ and A. L. Talapov, Zh. Eksp. Teor. Fiz. **75**, 1151 (1978) [Sov. Phys. JETP **48**, 579 (1978)].
[66]Yu. A. Izyumov and V. M. Laptev, Zh. Eksp. Teor. Fiz. **88**, 165 (1985) [Sov. Phys. JETP **61**, 95 (1985)].
[67]A. W. Overhauser, Phys. Rev. B **3**, 3173 (1971).
[68]P. A. Lee, T. M. Rice, and P. W. Anderson, Solid State Commun. **14**,

703 (1974).
[69]M. Steiner, Solid State Commun. **11**, 73 (1972).
[70]H. Yamazaki, E. A. Soares, H. Panepucci, and Y. Morishige, J. Phys. Soc. Jpn. **48**, 1453 (1980).
[71]M. Steiner, K. Kakurai, W. Knop, B. Dorner, R. Pynn, U. Happek, P. Day, and G. McLeen, Solid State Commun. **38**, 1179 (1981).
[72]P. A. Lindgard, J. Magn. Magn. Mater. **54–57**, 1227 (1986).
[73]R. S. Gekht, Zh. Eksp. Teor. Fiz. **91**, 190 (1986) [Sov. Phys. JETP **64**, 110 (1986)].
[74]C. J. Kroese, J. C. M. Tindemans-van Eyndhoven, and W. J. A. Maaskant, Solid State Commun. **9**, 1707 (1971).
[75]C. J. Kroese, W. J. A. Maaskant, and G. C. Verschoor, Acta Crystallogr. Sect. B **30**, 1053 (1974).
[76]B. S. Lee, J. Phys. C **12**, 855 (1979).
[77]K. Adachi, N. Achiwa, and M. Mekata, J. Phys. Soc. Jpn. **49**, 545 (1980).
[78]R. S. Gekht, Solid State Commun. **55**, 709 (1985).
[79]Y. Tazuke, H. Tanaka, K. Iio, and K. Nagata, J. Phys. Soc. Jpn. **50**, 3919 (1981).
[80]Yu. M. Gufan, Zh. Eksp. Teor. Fiz. **60**, 1537 (1971) [Sov. Phys. JETP **33**, 831 (1971)].
[81]I. E. Dzyaloshinskiĭ and B. G. Kukharenko, Zh. Eksp. Teor. Fiz. **70**, 2360 (1976) [Sov. Phys. JETP **43**, 1232 (1976)].
[82]D. Petitgrand, B. Hennion, P. Radhakrishna, C. Escribe, and S. Legrand, in: *Recent Developments in Condensed Matter Physics* (Proc. First General Conf. of Condensed Matter Division of European Physical Society, Antwerp, 1980, ed. by J. T. Devreese, L. F. Lemmens, V. E. Van Doren, and J. Van Royen), Vol. 4, Plenum Press, New York (1981), p. 205.
[83]K. L. Dudko, V. V. Eremenko, and V. M. Fridman, Zh. Eksp. Teor. Fiz. **68**, 659 (1975) [Sov. Phys. JETP **41**, 326 (1975)].
[84]A. S. Borovik-Romanov, M. P. Orlova, and P. G. Strelkov, Dokl. Akad. Nauk SSSR **99**, 699 (1954).
[85]E. Kanda, T. Haseda, and A. Otsubo, Physica (Utrecht) **20**, 131 (1954).
[86]V. M. Loktev, Fiz. Nizk. Temp. **5**, 295 (1979) [Sov. J. Low Temp. Phys. **5**, 142 (1979)].
[87]I. Yamada, K. Ubukoshi, and K. Hirakawa, J. Phys. Soc. Jpn. **54**, 3571 (1985).
[88]G. Sarma, Solid State Commun. **10**, 1049 (1972).
[89]J. Villain, J. Phys. C **6**, L97 (1973).
[90]R. S. Gekht and V. A. Ignatchenko, Zh. Eksp. Teor. Fiz. **76**, 164 (1979) [Sov. Phys. JETP **49**, 84 (1979)].
[91]P. W. Stephens, R. J. Birgeneau, C. F. Majkrzak, and G. Shirane, Phys. Rev. B **28**, 452 (1983).
[92]R. J. Meier and R. B. Helmholdt, Phys. Rev. B **29**, 1387 (1984).
[93]B. D. Metcalf, Phys. Lett. A **46**, 325 (1974).
[94]M. Kaburagi and J. Kanamori, Proc. Second Intern. Conf. on Solid Surfaces, Kyoto, 1974, in: Jpn. J. Appl. Phys. **13**, Suppl. 2, 145 (1974).
[95]H. Guth and G. Heger, in: *Fast Ion Transport in Solids* (Proc. Intern. Conf., Lake Geneva, WI, 1969, ed. by P. Vashishta *et al.*), North-Holland, Amsterdam (1979), p. 499.
[96]W. Press, B. Renker, H. Schulz, and H. Böhm, Phys. Rev. B **21**, 1250 (1980).
[97]M. Mekata, J. Phys. Soc. Jpn. **42**, 76 (1977).
[98]G. H. Wannier, Phys. Rev. **79**, 357 (1950).
[99]R. M. F. Houtappel, Physica (Utrecht) **16**, 425 (1950).
[100]G. H. Wannier, Phys. Rev. B **7**, 5017 (1973).
[101]J. V. José, L. P. Kadanoff, S. Kirkpatrick, and D. R. Nelson, Phys. Rev. B **16**, 1217 (1977).
[102]E. Müller-Hartmann and J. Zittartz, Z. Phys. B **27**, 261 (1977).
[103]K. Takasaki, I. Harada, and T. Tonegawa, J. Phys. Soc. Jpn. **55**, 4423 (1986).
[104]P. A. Slotte and P. C. Hemmer, J. Phys. C **17**, 4645 (1984).
[105]Y. Saito, J. Magn. Magn. Mater. **31–34**, 1049 (1983).
[106]B. Mihura and D. P. Landau, Phys. Rev. Lett. **38**, 977 (1977).
[107]D. P. Landau, Phys. Rev. B **27**, 5604 (1983).
[108]Y. Saito and G. Tabe, J. Phys. Soc. Jpn. **54**, 2955 (1985).
[109]Y. Saito, K. Furuta, and M. Hojou, J. Phys. Soc. Jpn. **56**, 178 (1987).
[110]S. Fujiki, K. Shutoh, Y. Abe, and S. Katsura, J. Phys. Soc. Jpn. **52**, 1531 (1983).
[111]B. D. Gaulin, M. F. Collins, and W. J. L. Buyers, J. Appl. Phys. **61**, 3409 (1987).
[112]H. Kadowaki, S. M. Shapiro, T. Inami, and Y. Ajiro, J. Phys. Soc. Jpn. **57**, 2640 (1988).
[113]Y. Ajiro, T. Nakashima, Y. Unno, H. Kadowaki, M. Mekata, and N. Achiwa, J. Phys. Soc. Jpn. **57**, 2648 (1988).
[114]S. H. Shenker and J. Tobochnik, Phys. Rev. B **22**, 4462 (1980).
[115]J. Villain, J. Phys. (Paris) **38**, 385 (1977).
[116]H. Kawamura, J. Appl. Phys. **61**, 3590 (1987).
[117]A. Z. Patashinskiĭ and V. L. Pokrovskii, *Fluctuation Theory of Phase Transitions*, Pergamon Press, Oxford, 1979 Russ., Nauka, M., 1975. Later eds. 1980 and 1982].
[118]A. E. Ferdinand and M. E. Fisher, Phys. Rev. **185**, 832 (1969).
[119]M. N. Barber, Phase Transitions Crit. Phenom. **8**, 145 (1983).
[120]D. P. Landau, Phys. Rev. B **14**, 255 (1976); **16**, 4164 (1977).
[121]P. I. Belobrov, R. S. Gekht, and V. A. Ignatchenko, Zh. Eksp. Teor. Fiz. **84**, 1097 (1983) [Sov. Phys. JETP **57**, 636 (1983)].
[122]K. Takeda, N. Uryu, K. Ubukoshi, and K. Hirakawa, J. Phys. Soc. Jpn. **55**, 727 (1986).
[123]H. Kadowaki, K. Ubukoshi, K. Hirakawa, J. L. Martinez, and G. Shirane, J. Phys. Soc. Jpn. **56**, 4027 (1987).
[124]D. R. T. Jones, A. Love, and M. A. Moore, J. Phys. C **9**, 743 (1976).
[125]J. C. Le Guillou and J. Zinn-Justin, Phys. Rev. Lett. **39**, 95 (1977).
[126]I. Ono and T. Oguchi, Phys. Lett. A **38**, 39 (1972).
[127]H. Kawamura and S. Miyashita, J. Phys. Soc. Jpn. **54**, 4530 (1985).
[128]S. Miyashita, J. Phys. Soc. Jpn. **55**, 3605 (1986).
[129]L. G. Marland and D. D. Betts, Phys. Rev. Lett. **43**, 1618 (1979).
[130]T. Oguchi, H. Nishimori, and Y. Taguchi, J. Phys. Soc. Jpn. **55**, 323 (1986).
[131]P. Fazekas and P.W. Anderson, Philos. Mag. **30**, 423 (1974).
[132]M. Imada, J. Phys. Soc. Jpn. **56**, 311 (1987).
[133]F. Y. Wu, Rev. Mod. Phys. **54**, 235 (1982).
[134]H. Kawamura, J. Appl. Phys. **63**, 3086 (1988).

Translated by A. Tybulewicz